2020•2021

Faculteit Industriële Ingenieurswetenschappen

master in de industriële wetenschappen: nucleaire technologie

Masterthesis

A new eff measurement system using the Californium Source Method

PROMOTOR :

Prof. dr. Jan WAGEMANS

PROMOTOR :

Dr. Anatoly KOCHETKOV

BEGELEIDER :

PhD. Antonin KRASA

Lena Matthys

Scriptie ingediend tot het behalen van de graad van master in de industriële wetenschappen: nucleaire technologie, afstudeerrichting nucleaire en medisch

Gezamenlijke opleiding UHasselt en KU Leuven

2020•2021

Faculteit Industriële Ingenieurswetenschappen

master in de industriële wetenschappen: nucleaire technologie

Masterthesis

A new eff measurement system using the Californium Source Method

PROMOTOR :

Prof. dr. Jan WAGEMANS

PROMOTOR :

Dr. Anatoly KOCHETKOV

BEGELEIDER :

PhD. Antonin KRASA

Lena Matthys

Scriptie ingediend tot het behalen van de graad van master in de industriële wetenschappen: nucleaire technologie, afstudeerrichting nucleaire en medisch

UHASSELT KU LEUVEN

ACKNOWLEDGEMENTS

Before proceeding with this Master's thesis itself, I would like to thank several people. First of all, I would like to thank everyone at SCK CEN who helped me during the writing of my Master's thesis.

I would like to thank Dr. Jan Wagemans for the opportunity to work with SCK CEN on this topic and his continuous guidance and feedback on my work.

Next, I would like to thank Dr. Anatoly Kochetkov for teaching me the procedures and his support during the experiments.

Also, a special thanks to PhD. Antonin Krasa for following the progress of my work closely. Thank you for answering every question I had and helping me every turn of the way.

Finally, I would like to thank my parents who have supported me unconditionally during the past years and made these studies possible.

TABLE OF CONTENTS

LIST OF TABLES

LIST OF FIGURES

LIST OF SYMBOLS

α	Prompt neutron decay constant
β	Delayed neutron fraction
β_{eff}	Effective delayed neutron fraction
β_i	Delayed neutron fraction of the ith group
λ	Radioactive decay constant
$\bar{\nu}$	Average number of neutrons emitted per fission
ρ	Reactivity
σ	Microscopic cross section
τ_d	Dead-time of a detector
τ_e	Reactor period
τ_i	Mean precursor lifetime of the ith group
ϕ	Neutron flux
Φ^*	Adjoint flux of importance function
Λ	Prompt neutron generation time or mean generation time
Σ	Macroscopic cross section
Ω	Direction of the neutron
$a_{i,eff}$	The relative abundances of precursor groups
f	Conversion factor between the central fission rate and the fission rates in the whole reactor
$f_{dead\text{-}time}$	Correction factor to include the dead-time
k_{eff}	Effective multiplication factor
l	Prompt neutron lifetime
l_d	Mean generation time with delayed neutrons
m	Measured count rate
n	Neutron density
r	Position of the neutron
t_d	Diffusion time
t_s	Slowing down time
v	Neutron velocity
A_t	Activity at time t
E	Neutron energy
I	Importance factor
N	Atomic number density
P_t	The probability to measure correlated and uncorrelated neutrons
Q_{Cf}	Fission rate
S_{Cf}	Strength of the californium source
$T_{1/2}$	Half-life
RR	Reaction rate.

ABSTRACT

SCK CEN, the national research center on nuclear energy located in Mol, has a zero-power reactor VENUS-F that supports the realization of the MYRRHA Accelerator Drive System. VENUS-F is used to verify calculation codes and nuclear data for MYRRHA. Research with VENUS-F provides an insight into the time-dependent behavior of a nuclear reactor by experimentally determining kinetic parameters.

This Master's thesis focuses on the determination of the delayed neutron fraction β_{eff} with the Californium Source Method. In addition, the neutron noise method (the Rossi-α method) is performed to determine the mean neutron generation time Λ. For this purpose, firstly an application system is devised to perform the β_{eff} measurements using the Californium Source Method. Next, the experimental data are analyzed. Finally, Serpent2, which is based on Monte Carlo simulations, is used to determine correction factors that are necessary for the Californium Source Method. In addition to the measurement of the β_{eff} and Λ values, their uncertainties are also determined.

The measurement system, consisting of the californium source attached to a remotely controlled moving mechanism, fission chamber with calibrated effective mass, neuron flux monitors and data acquisition system was successfully tested.

ABSTRACT IN NEDERLANDS

SCK CEN, het nationaal studiecentrum voor kernenergie te Mol, beschikt over een nulvermogen reactor VENUS-F waarmee dat de realisatie van MYRRHA *Accelerator Driven System* ondersteunt. VENUS-F wordt gebruikt om berekeningscodes en nucleaire data te verifiëren. Onderzoek met VENUS-F geeft inzicht in het tijdafhankelijk gedrag van een kernreactor door experimenteel kinetische parameters te bepalen.

Deze masterscriptie focust op het bepalen van de vertraagde neutronenfractie β_{eff} met de Californium bron methode. Daarnaast wordt ook de neutron ruis methode (de Rossi-α methode) uitgevoerd om de gemiddelde neutron generatietijd Λ te bepalen. Hiervoor wordt eerst een mechanisch systeem ontworpen om de β_{eff}-metingen met de Californium bron methode uit te voeren. Vervolgens worden de experimentele data geanalyseerd. Ten slotte worden met behulp van Serpent2, dat gebaseerd is op Monte Carlo simulaties, correctiefactoren bepaald die nodig zijn voor de Californium bron methode. Naast de berekening van β_{eff} en Λ worden ook hun onzekerheden bepaald.

Het meetsysteem, bestaande uit de californiumbron bevestigd aan een op afstand bediend bewegend mechanisme, een splijtingskamer met gekalibreerde effectieve massa, neuronfluxmonitors en een data-acquisitie systeem werd met succes getest.

1 INTRODUCTION

SCK CEN is the national research center on nuclear energy of Belgium, which has been located in Mol since its foundation in 1952. SCK CEN started with one research reactor BR1 but has since then expanded its activities to various other sectors such as radiobiology, radio-ecology and astronautics [1].

In 1964 the research reactor VENUS, which stands for Vulcan Experimental NUclear Study, was commissioned. VENUS is a flexible experimental reactor with a maximal thermal power of 500 Watt making it a "zero-power" reactor. VENUS is mainly used for validation of reactor physics calculation codes. In 2008 VENUS was re-built as a fast lead-based reactor to support research in Accelerated Driven Systems (ADS) and in the Multi-purpose HYbrid Research Reactor for High-tech Applications (MYRRHA)[1].

Experimental research with VENUS provides insight into the time-dependent behavior of a nuclear reactor, which is determined by kinetic parameters. The most important kinetic parameters are the effective delayed neutron fraction (β_{eff}), and the mean neutron generation time (Λ). β_{eff} expresses the share of delayed neutrons among all fission neutrons in the reactor. Λ is the average time from neutron production until absorption inducing fission. The kinetic parameters depend on the type of fuel and on the neutron spectrum (influenced by the geometry and the materials of a specific reactor core configuration).

1.1 PROBLEM STATEMENT

The MYRRHA reactor is a new concept reactor whose design is under development, for which it is important to test the calculation tools. VENUS-F coupled to a particle accelerator is a mock-up of MYRRHA. Its tasks are to develop a sub-criticality measurement technique and to verify calculation codes and nuclear data for MYRRHA.
Thus, the main goal of VENUS-F is to support design development and licensing of the MYRRHA project. For the complete experimental characterization of new reactor designs, the measurement of β_{eff} and neutron importance function are necessary.

1.2 OBJECTIVE

The goal of the proposed study is to create a measurement system for the application of the β_{eff} measurements using the Californium Source Method at the VENUS-F reactor. This means to design and construct a remote-controlled mechanism for insertion of the ^{252}Cf source and to perform a set of measurements. Next the experimental data from the neutron detectors (^{235}U fission chambers) need to be analyzed to determine the β_{eff} value and the spatial distribution of the neutron importance function. The neutron importance function describes the "importance" or "worth" of a neutron for causing fission (so-called adjoint flux Ø*) as a function of neutron position *r*, direction Ω and energy *E*. Additional measurements using the neutron noise technique (the Rossi-α method) will enable to determine $\alpha = \beta_{eff}/\Lambda$ and Λ. Monte Carlo simulations (Serpent2 or MCNP6) will be carried out to calculate correction factors needed for the Californium Source Method. Furthermore, it is crucial to thoroughly determine the experimental uncertainties.

2 REACTOR PHYSICS

Before building a nuclear reactor, it is important to know the time-dependent behavior of the neutron population in the reactor. This time-dependent behavior of a reactor is in fact the reaction of the reactor to a planned or unplanned event that causes a change in the reactivity of the reactor. Which in turn leads to changes in the neutron flux, and thus the reactor power [2].

2.1 NEUTRON FLUX

The neutron flux ϕ (neutrons*cm^{-2}*s^{-1}) expresses the total distance all neutrons in a unit volume can travel each second. It is determined by the velocity of the neutrons v (cm*s^{-1}) and the neutron density n (neutrons*cm^{-3}), which represents the number of neutrons that exist in one cubic centimeter [2]:

$$\phi = n * v\,. \tag{1}$$

The neutron flux is a scalar quantity meaning that the neutrons are not subjected to a specific direction[2]. A nuclear reactor consists of many different parts made from different materials. A neutron will interact differently according to the material and thus the different materials can influence the neutron flux or neutron diffusion. Additionally, the energy of the incoming neutron affects the type of reaction (e.g. scatter, absorption) the neutron will undergo. This makes that the neutron flux is defined by a set of differential equations with several variables.

Not every neutron has the same weight with respect to the multiplicity of the system. The spatial direction and the energy of the neutron matter. A neutron at the core periphery that is directed outwards, will not contribute equally to the multiplication system as a neutron in the center of the reactor core. Therefore, an importance function, also called adjoint flux, of a neutron causing fission is often determined.
Physically[1], the adjoint flux, ϕ*(**r**, E, **Ω**), expresses the probability of a neutron at position r, with direction Ω and energy E to induce fission inside the reactor [3].

It is essential to know that the importance is only meaningful for a critical reactor. This can be explained based on the physical meaning of the importance function. It represents a proportionality to the total number of neutrons produced by introducing a neutron at position r, with energy E and a direction Ω. Suppose one has a supercritical reactor, the value will be infinitely large, while with a subcritical reactor the value will be zero.

[1] Besides the physical meaning it has a mathematical meaning, which is the reason why it is called "adjoint flux". The adjoint matrix is in fact the conjugate transpose matrix. It represents a matrix that had complex entries in its original matrix as a symmetric matrix with real values as entries. This means that the entry in row I and column J is equal to its real value in row J and column I in the adjoint matrix. In addition, the adjoint matrix has the condition that it satisfies boundary conditions which state that the initial conditions are equal to the finite conditions [29].

2.1.1 Reaction rate

The reaction rate, which is related to the reactor power, (interactions*cm^{-3}s^{-1}) is given by the neutron flux and the macroscopic cross section Σ, which expresses the probability of an interaction per centimeter path length (interactions*cm^{-1}). Thus, the reaction rate gives the number of interactions in one cubic centimeter in one second.

$$RR = \int_0^\infty \phi(\mathrm{E}) * \Sigma(\mathrm{E}) dE = \int_0^\infty \phi(E) * N * \sigma(E) dE \tag{2}$$

The macroscopic cross section can be expressed by the atomic number density N (atoms*cm^{-3}) multiplied by the microscopic cross section σ (cm^2) [2]. Note that the reaction rate is expressed as an integral of the energy. This is because the cross section and the neutron flux are dependent on the energy. Thus, only if one works with mono-energy neutrons is the integral omitted from the equation.

2.2 THE EFFECTIVE MULTIPLICATION FACTOR

The time-dependent behavior of a reactor is determined by kinetic parameters such as β_{eff} and Λ. To understand these kinetic parameters, one must first understand the environment in which a reactor operates.

A fission reaction can occur when a neutron is absorbed by a heavy target nucleus, creating a compound nucleus. If the excitation energy of the compound nucleus is greater than the critical energy, the nucleus splits into two fission fragments. In addition to these two fission fragments, a large amount of energy and 2-3 free neutrons are released. The free neutrons will subsequently also interact with other nuclei, which may or may not induce further fissions. Depending on the conditions of the multiplication environment the chain reaction evolves. This multiplication system can be described with the effective multiplication factor k_{eff} [2].

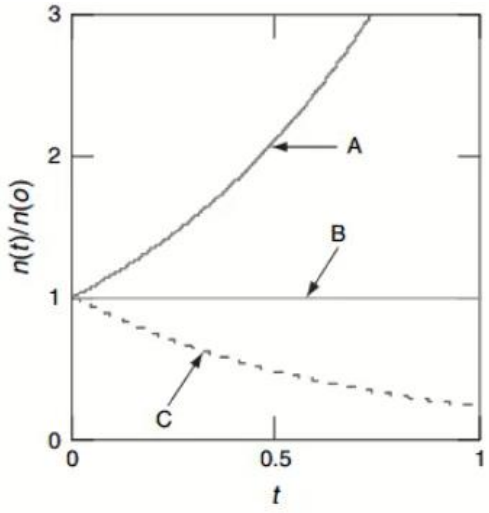

Figure 1: Change in the neutron population for a reactor in A- a supercritical state, B- a critical state and C- a subcritical state [2].

The multiplication factor (k_{eff}) describes the ratio of the fission neutron population in one generation to the neutron population of the previous generation [2]. If k_{eff} is greater than one, the system is supercritical and the multiplication system, and thus the reactor power, increases

exponentially [3], [4]. When k_{eff} is less than 1, the neutron population will decrease in time meaning the chain reaction will not be sustained. Ideally, the k_{eff} of a reactor should be equal to 1, the reactor is critical, which means there is no change in the neutron population in time and the chain reaction is self-sustaining [2]. Figure 1 shows that in a supercritical and respectively subcritical reactor state, the neutron population will increase (line A) and decrease (line C) exponentially. While for a critical reactor, the neutron population will remain constant over time and the k_{eff} is equal to 1 (line B). However, the multiplication factor cannot be directly measured.

2.2.1 The reactivity

Another quantity derived from the multiplication factor, the reactivity ρ, is used to determine how far the reactor is from criticality. The reactivity ρ is defined as:

$$\rho = \frac{k_{eff} - 1}{k_{eff}}. \tag{3}$$

Since k_{eff} is dimensionless, the reactivity ρ is also dimensionless, furthermore ρ is often expressed in pour cent mille or hundred-thousandths (pcm = 10^{-5}) [3]. However, if ρ is normalized to the delayed neutron fraction, which will be explained further on, it is expressed in dollars ($). When ρ is normalized it indicates the departure from a prompt critical reactor state. This is useful because it states the exact response the reactor will have on a reactivity insertion [2].

As stated in Table 1, ρ will be equal to zero if the reactor is critical. Thus, the larger the absolute value of ρ, the more the reactor deviates from criticality [2]. The reactivity can be adjusted by using control systems, such as neutron absorbing control rods. When a control rod is inserted in the reactor, more neutrons will be absorbed by the control rod and consequently not induce fission. The neutron population will decrease in time meaning that k_{eff} will be less than 1. The movement of the control rod caused an insertion of a negative reactivity and the reactor will become subcritical.

2.2.2 The reactor period

The reactivity cannot be directly measured, therefore a different way to estimate the reactivity is used. A quantity, namely the reactor period τ_e (s), is determined experimentally as the change in reactor power in time. It is defined as the time needed for the neutron density to change by a factor e = 2.718. Furthermore, equation (4) shows that the neutron density can be calculated from the initial neutron density and the reactor period:

$$n_t = n_0 * e^{\frac{t}{\tau_e}}. \tag{4}$$

If the reactor is critical, the current neutron density needs to be equal the initial neutron density, which means that the exponent has to be equal to 1. Hence, the reactor period should be equal to infinity, which is shown in Table 1. This means that it will take infinite time for the reactor period to change the neutron density with a factor e. Table 1 also shows that if the reactor is subcritical, this is when k_{eff} is smaller than 1, the reactor period is negative. Thus, the reactor power will be decreasing. On the other hand, if the reactor period is positive, the reactor power will increase, and the reactor is supercritical. If the reactor period is associated with an exponential power change, it is also referred to as the stable or asymptotic reactor period.

Table 1: Values for the multiplication factor, the reactivity and the reactor period for a subcritical, critical and supercritical reactor.

Reactor State	k_{eff}	ρ	τ_e
Subcritical	<1	<0	<0
Critical	=1	=0	∞
Supercritical	>1	>0	>0

2.3 PROMPT VERSUS DELAYED NEUTRONS

It was mentioned that usually 2 or 3 free neutrons are emitted during fission of a heavy nucleus, which is shown in Figure 2 on examples of ^{235}U, ^{238}U and ^{239}Pu. The graph also shows that with a higher energy of the incident neutron, more neutrons will be emitted during fission. In addition, ^{239}Pu will generally emit more neutrons than ^{235}U and ^{238}U. In addition to the neutrons that are emitted immediately upon fission (as shown in Figure 2), neutrons can also be emitted later after fission. Fission neutrons can thus be divided into two groups: prompt neutrons and delayed neutrons.

Delayed neutrons are emitted by neutron rich fission fragments with a delay of the order of seconds and minutes after the fission event [2]. The neutron rich fission fragments mainly undergo β^--decay and if a nucleus in the β^--decay chain is excited beyond the binding energy of a neutron, a neutron can be emitted [3]. Figure 3 shows the production of delayed neutrons by fission products of ^{235}U, ^{238}U and ^{239}Pu. The graph shows that there is little change in the number of delayed neutrons produced by the fission fragments if the incident neutron has an energy below 2 MeV. The fission fragments that can emit a neutron, are called the delayed neutron precursors. Comparing Figure 2 and Figure 3, it also shows that the amount of delayed neutrons produced is two orders of magnitude less than the amount of prompt neutrons produced.

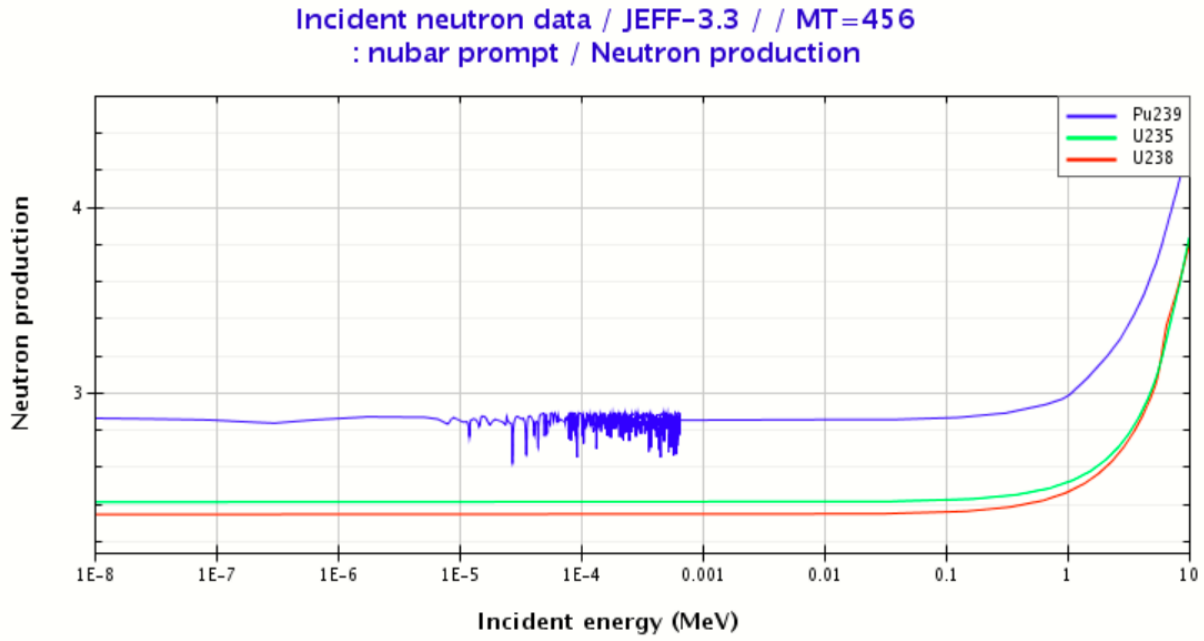

Figure 2: Production of prompt neutrons from fission of ^{235}U, ^{238}U and ^{239}Pu according to the energy of the incoming neutron [5].

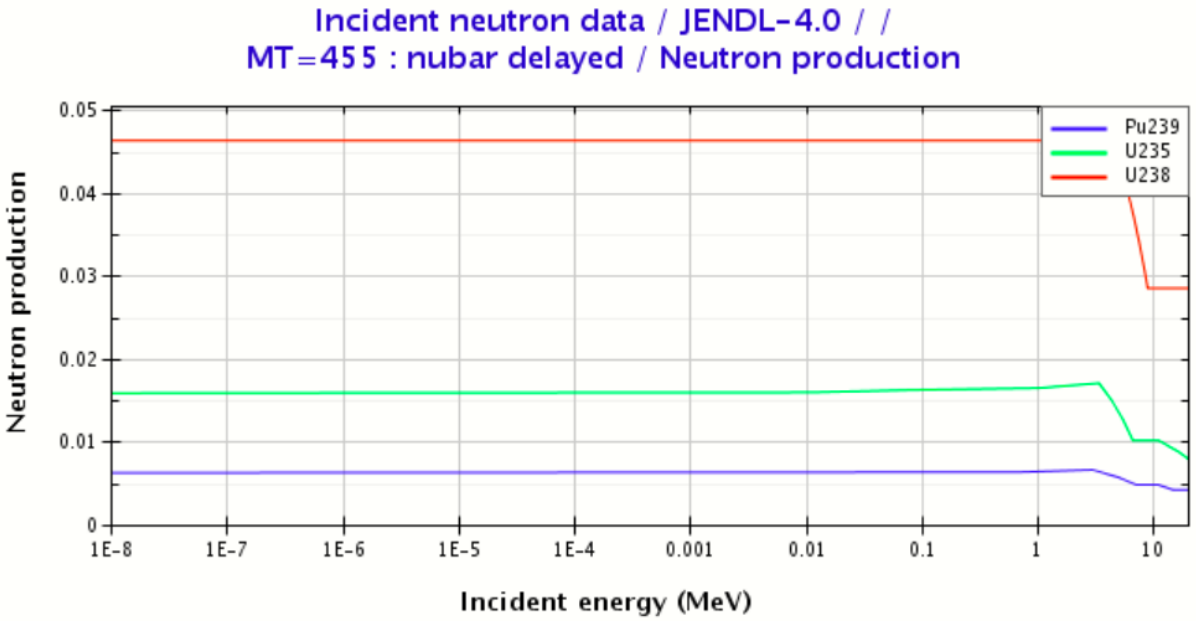

Figure 3: Production of delayed neutrons by fission products of ^{235}U, ^{238}U and ^{239}U according to the energy of the incoming neutron [5].

Figure 4 and Figure 5 show the energy distribution of the delayed neutrons and prompt neutrons which are emitted during fission of ^{235}U, ^{238}U and ^{239}Pu, respectively. The average energy of a delayed neutron is 0.4 MeV. The average energy and the most probable energy of a prompt neutron is 2 MeV and 0.7 MeV, respectively [2]. Note that the prompt neutron spectrum displays a continuous energy spectrum. The delayed neutron spectrum contains peaks that indicate the reason lies in discrete energy levels of the fission product.

Prompt neutrons are emitted within a very short time ($\sim 10^{-14}$ seconds) directly from fission and make more than 99% of the neutrons produced in fission. Although only less than 1% of the fission neutrons are delayed neutrons, they play a crucial role in reactor control and thus for reactor safety. Delayed neutrons change the dynamic time response of the reactor, making it controllable by control systems such as control rods [2].

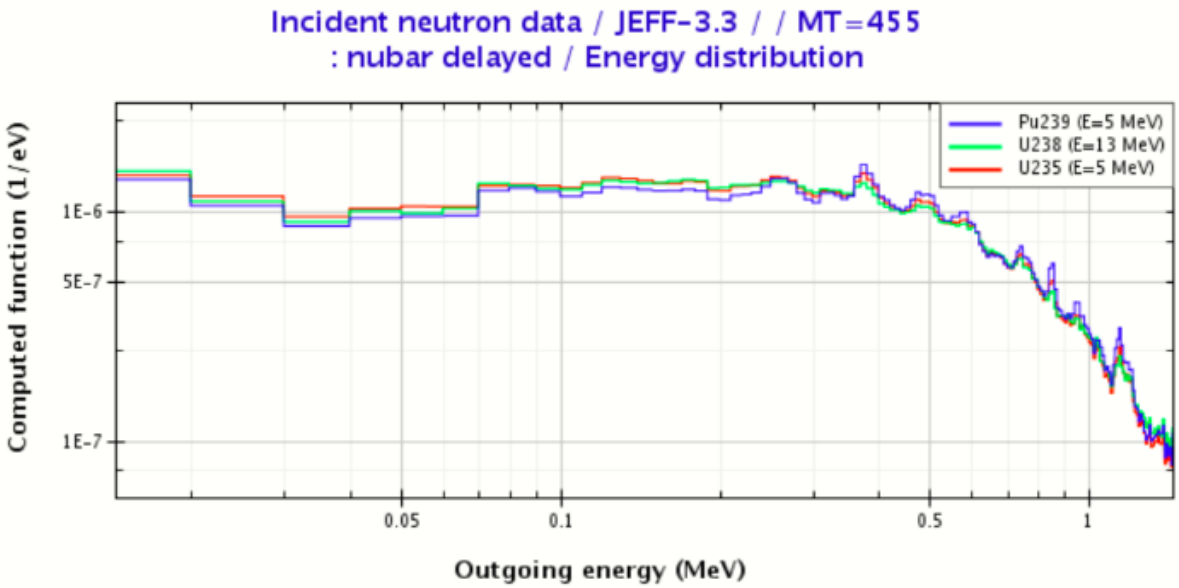

Figure 4: Energy distribution of the delayed neutrons emitted by fission products of ^{235}U, ^{238}U and ^{239}Pu [5].

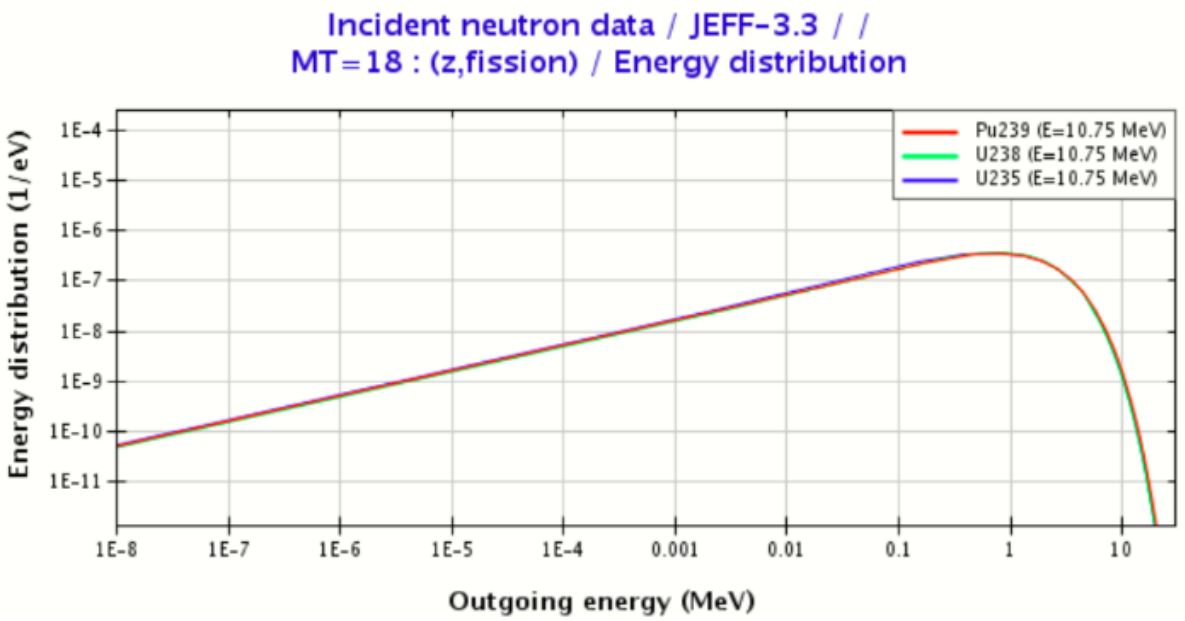

Figure 5: Energy distribution of the prompt neutrons emitted as a result of fission of ^{235}U, ^{238}U and ^{239}Pu [5].

2.3.1 The effective delayed neutron fraction

There are about 240 precursors [2], which is too much for reactor kinetics calculations to be performed for each individual precursor in a reasonable time. Therefore, they are subdivided into six or eight delayed neutron groups according to their half-lives $T_{1/2}$. This means that neutrons originating from a decay of precursors with similar half-life are classified as belonging to one delayed neutron group [3]. An average half-life is calculated for each group.
The delayed neutron fraction β is the ratio of the number of delayed neutrons to the number of all the fission neutrons (i.e. the sum of the prompt neutrons and delayed neutrons):

$$\beta = \frac{\text{delayed neutrons}}{\text{prompt neutrons}+\text{delayed neutrons}}. \tag{6}$$

The delayed neutron fraction β depends on the fissioning isotope and on the incident neutron energy. Thus, depending on the type of reactor (e.g. thermal or fast), delayed neutrons are more or less effective than prompt neutrons. For example, delayed neutrons have a lower average energy (0,4 MeV) than prompt neutrons (2 MeV). To include this effect the effective delayed neutron fraction β_{eff} is defined:

$$\beta_{eff} = \beta * I. \tag{7}$$

Here, the importance factor I states the effectiveness of the neutrons. The energy distribution of the delayed neutrons differs from group to group and thus every group will have different effectiveness. Therefore, if necessary, a concept of the importance function or the adjoint flux ϕ^* is introduced which gives different importance to the different energy groups. The adjoint flux can be calculated to include the probability of a neutron at position r with energy E inducing fission in the reactor [2], [3].

2.3.2 Mean neutron generation time

The prompt neutron generation time (or mean generation time) Λ (s), is the average time between the birth of the neutron by fission and its capture resulting in fission. The mean generation time can be written as followed:

$$\Lambda = \frac{l}{k_{eff}}. \tag{8}$$

The parameter l is the prompt neutron lifetime, which is the average time between the birth of the neutron by fission and its absorption or its escape from the system. The prompt neutron lifetime can be expressed as the sum of the slowing down time and the diffusion time. The slowing down time is the mean time needed for the fission neutrons to slow down to thermal energies. This process is also called neutron thermalization. The diffusion time is expressed as the average time thermal neutrons have to diffuse before they are lost [7]:

$$l = t_s + t_d. \tag{9}$$

In a fast reactor there are both thermal and fast neutrons but because the neutron thermalization of fast neutrons is suppressed, the prompt neutron lifetime is much shorter. It has a typical value of the order of 10^{-7}

3 THE VENUS-F REACTOR

3.1 DESCRIPTION OF THE VENUS-F REACTOR

The VENUS-F reactor is placed in an open-top stainless-steel cylindrical vessel with a radius of approximately 80 cm and a height of 140 cm. Figure 6 shows that the reactor core consists of a 12 x 12 square lattice of assemblies, thus containing 144 elements. The core is surrounded by stainless-steel (green) and top, bottom and radial reflectors made out of lead (blue) [8], [9].

Every assembly can be filled with fuel, reflector material (Pb or C), B_4C or any other material. The assemblies containing B_4C, which is a neutron absorbing material, are control rods (CR) or safety rods (SR). Safety rods consist of B_4C but also have a fuel follower. Fuel assemblies have a 5 x 5 grid and are composed of 30 wt% enriched uranium (i.e. 30% of the metallic uranium consist of ^{235}U), solid lead or bismuth and Al_2O_3 (see Figure 7). The lead-bismuth mixture is to simulate the liquid coolant and Al_2O_3 is to simulate the MOX fuel (oxide fuel) that will be used in MYRRHA. Besides the different materials, an assembly can also contain a guiding tube, which serves as an experimental channel to insert detectors. Guiding tubes penetrate the top reflector and, in some cases, can go as far as into the bottom reflector [8], [9].

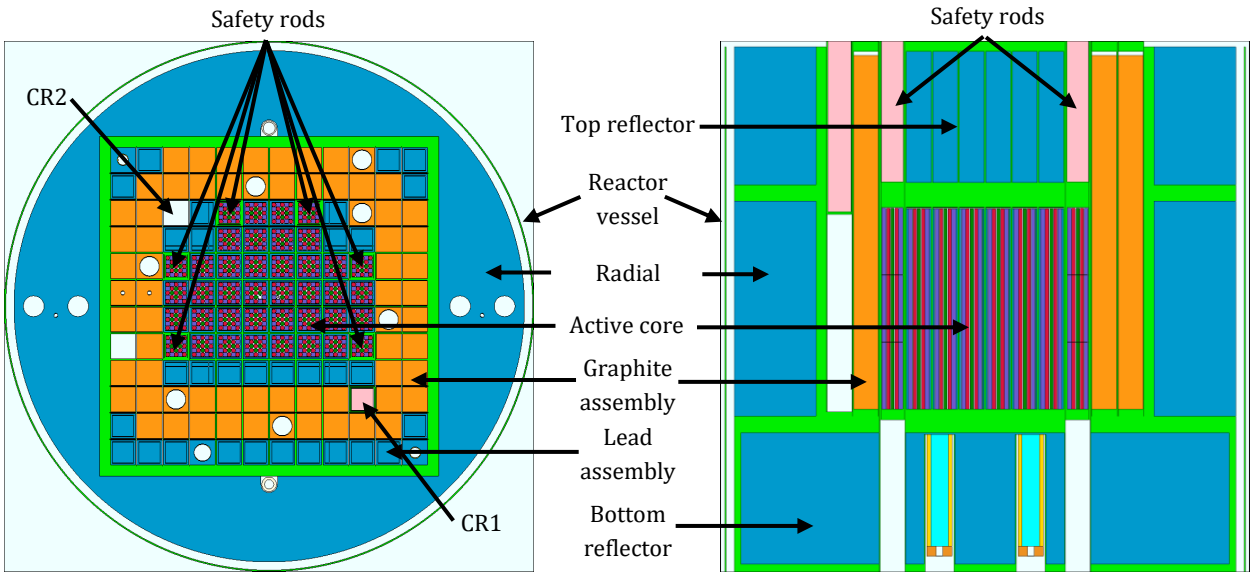

Figure 6: Radial (left) and axial (right) view of VENUS-F with core composition CC12. The colors represent the following materials: blue – lead, orange – graphite, pink – B_4C, red – uranium, purple – bismuth, olive green – Al_2O_3, light green – stainless steel, white - air.

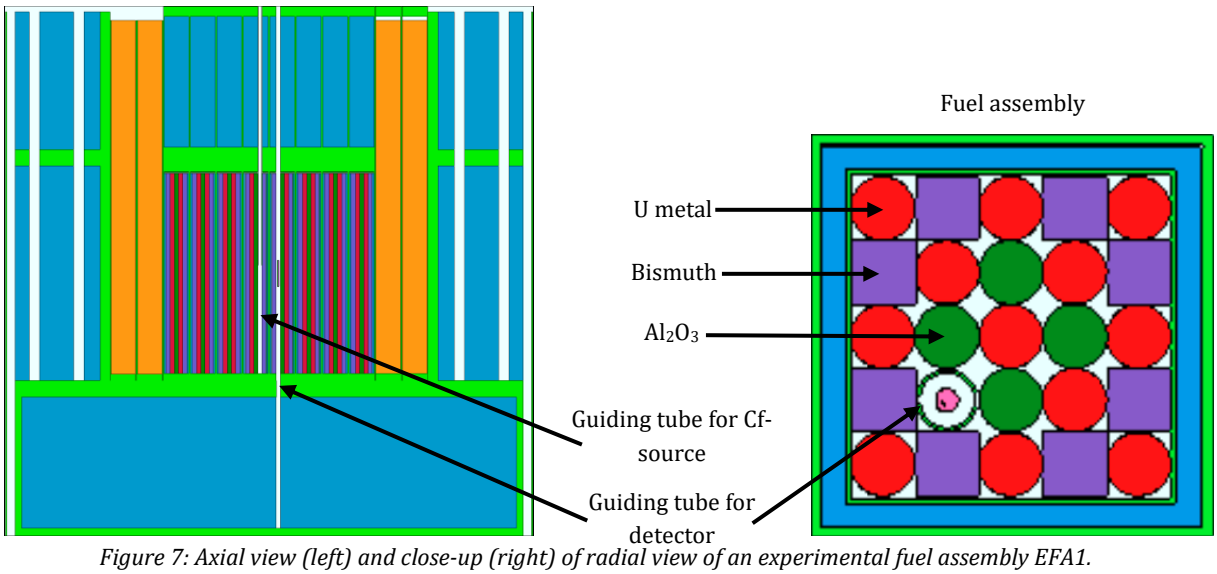

Figure 7: Axial view (left) and close-up (right) of radial view of an experimental fuel assembly EFA1.

3.2 External neutron source

When the reactor is in a subcritical state, various extraneous neutron sources can be used, which emit neutrons other than prompt or delayed neutrons from neutron-induced fission (e.g. alpha-neutron sources, high-energy gamma-neutron sources, or accelerator-based neutron generators). In this work, ^{252}Cf, which undergoes spontaneous fission producing fission fragments and emitting free neutrons, will be used [2], [10]. Figure 8 shows that the emitted neutrons have a fast energy spectrum with an average energy of 2.1 MeV and a most probable energy of 0.7 MeV [11].

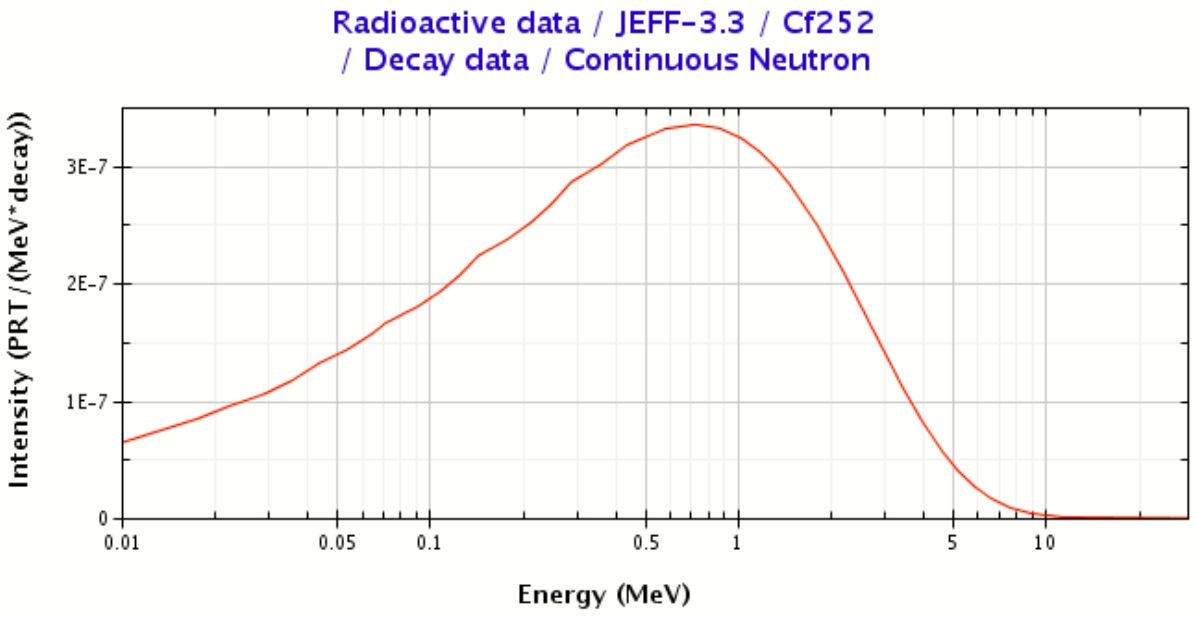

Figure 8: Energy spectrum of the neutrons emitted by spontaneous fission of ^{252}Cf [5].

3.3 MEASUREMENT OF NEUTRONS

Neutrons are electrically neutral particles therefore they are not directly ionizing. Thus, to measure neutrons they must first be converted into charged particles after which they can be measured with conventional radiation detectors. One way to convert neutrons into charged particles is by absorption. The neutron will be absorbed by a converter material, such as ^{10}B or ^{235}U, which on their turn will emit secondary particles, such as alpha and beta particles, photons or fission products. Afterwards the secondary particles can be measured, for example with an ionization chamber.

A ^{235}U fission chamber (see Figure 9) is an ionization chamber with a thin layer of ^{235}U (for example on the wall), which is used as converter material. The thin layer will produce fission fragments if a neutron is absorbed by ^{235}U. These fission fragments are heavy charged particles with a high kinetic energy and will create a signal in the ionization chamber [12].

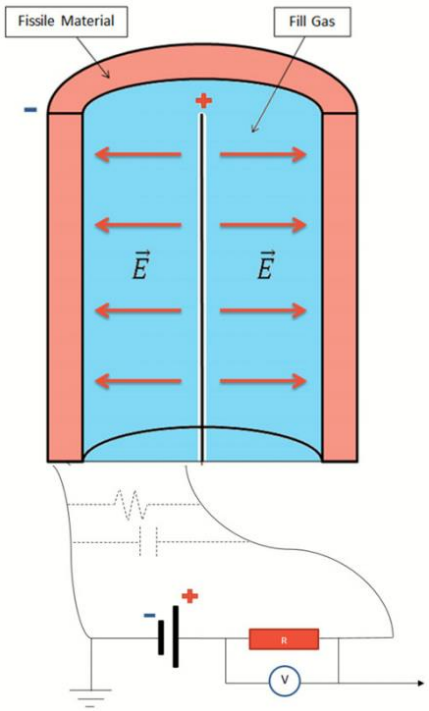

Figure 9: Schematic view of a typical fission chamber [12, p. 2].

An ionization chamber is composed of a chamber filled with a noble gas, such as argon, and two polarized electrodes. A voltage is applied between the electrodes, which creates an electrical field between the cathode and anode. When the fission chamber is positioned in a neutron flux, neutrons will induce fission in the ^{235}U layer, which will produce two fission fragments and some neutrons. The fission chamber is designed such that at least one fission fragment will travel into the gas inside the chamber and will ionize the gas, creating ions and electrons, along its track. The fission fragments have a high kinetic energy and will deposit most of their energy to the gaseous atoms. Because of the electric field between the anode and the cathode, free electrons will move to the anode and will be collected on the wire. This produces a signal in the form of an electrical current or pulse[2], [12], [13].

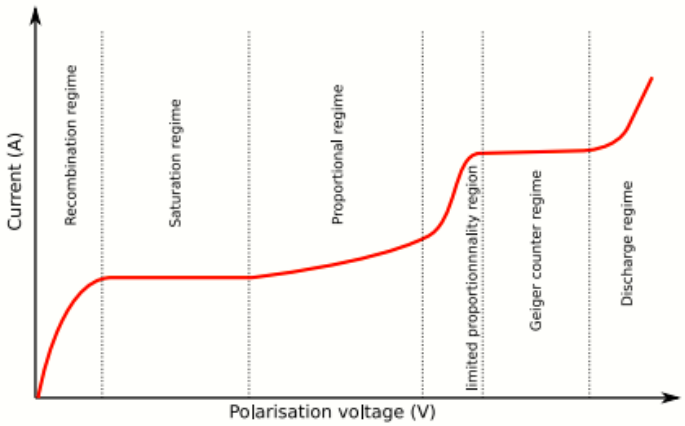

Figure 10: Operation regimes of an ionization chamber [13, p. 2].

Figure 10 shows the different regimes an ionization chamber can work under depending on the voltage applied to the anode and cathode. In the recombination regime, ions and electrons tend to recombine. This leads to an underestimation because not every ion-pair that is created will be collected. Next, at higher voltage, the saturation regime is reached [13]. Here the number of ion-pairs collected by the electrodes is equal to the number of ion-pairs created by the fission fragments [2]. This is also the region where fission chambers usually operate in. If the voltage is further increased, the charges, created by the ionization of the gas, themselves can induce secondary ionization. This process is called avalanche multiplication and it creates a proportional output to the deposited energy. Therefore, this region is called proportional regime. After this regime, the proportionality is no longer guaranteed as a cloud of positively charged ions form a cloud between the electrodes and reduce the effect of the electric field. This limited proportionality region is then followed by the Geiger-Mueller, where it is again possible to measure each individual incident particle. Lastly, the detector undergoes continuous discharge, which can damage the detector. Naturally, the detector should not be working in this regime [14].

In addition to the voltage at which an ionization chamber can operate, it can also operate in three different modes. The first mode is the pulsed mode, where it is possible to detect every signal or pulse separately. This mode is used in low neutron fluxes. Secondly, there is the current mode where the different counts are not measured separately but the entire current is measured. The current is proportional to the neutron flux. This mode is mainly used in high neutron fluxes such as in a nuclear power plant reactor or a high-flux research reactor. Lastly, in the Campbell mode there is a pile up from pulses that prevents measuring every pulse separately. However, it is still possible to distinguish pulses by looking at fluctuations in the current [13].

When measuring the count rate with an ionisation chamber, one must take into account the dead time τ_d. This is the time after an event in which the detector cannot register any pulses. This is especially an important phenomenon for detection of high neutron fluxes and therefore high detector count rates [2]. The measured count rate m can be corrected with a non-paralyzable dead-time correction factor [14]:

$$f_{dead-time} = \frac{1}{1 - m * \tau_d}. \tag{11}$$

4 METHODS FOR MEASURING KINETIC PARAMETERS

There are different experimental methods to measure kinetic parameters such as those using the neutron source or neutron noise techniques [15]. This section discusses the principles of the methods to be used at the VENUS-F reactor, which are based on the californium source method supplemented with the Rossi-α neutron noise method.

4.1 THE CALIFORNIUM SOURCE METHOD

The Californium Source Method uses following equation to determine β_{eff}:

$$\beta_{eff} = \frac{S_{Cf}}{|\rho_\$| * Q_f * \bar{\nu}} * \frac{1}{f} * \frac{F^+_{\chi,Cf}(0)}{\overline{F^+_\chi}}. \quad (12)$$

Where:

- S_{Cf} strength of the inserted ^{252}Cf source,
- $|\rho_\$|$ subcriticality in β_{eff} units,
- $\bar{\nu}$ reactor-averaged number of neutrons emitted per fission,
- Q_f changing of a fission rate, measured by the absolute fission chamber, due to ^{252}Cf source insertion into the core center at $\rho_\$$
- f conversion factor between the central fission rate measured by the absolute fission chamber and the fission rates in the whole reactor,
- $\frac{F^+_{\chi,Cf}(0)}{\overline{F^+_\chi}}$ ratio of the introduced ^{252}Cf neutron importance at the core center to reactor averaged neutron importance [16, p. 143].

The californium source method was developed by S. Carpenter, J. Gasidlo and J. Stevenson in the Argonne National Laboratory in Idaho in 1971. Carpenter and co wanted to determine the effective delayed neutron fractions of ^{235}U and ^{239}Pu for two fast critical assemblies. They wanted to examine whether the experimental values corresponded with calculations. It could be concluded that earlier received discrepancies of 30% in measured and calculated reactivity values in fast critical experiments were not caused by erroneous delayed neutron data [17]. Later on, this method was used by E. Fischer and T. Sakurai and S. Okajima on different fast critical reactor cores [18], [19].

To solve equation (12), first the core reactivity is determined, for example using calibrated control rods. Next, the change in the fission rate Q_f is experimentally determined. Then, the strength of the source is calculated to the date on which it is used. Lastly, the parameters $\bar{\nu}$, f and $F^+_{\chi,Cf}(0)/\overline{F^+_\chi}$ from equation (12) are calculated using Monte Carlo or deterministic codes.

4.1.1 The calibration of control rods

The measurement of the reactivity is based on the measurement of the asymptotic period or the stable reactor period τ_e. By pulling the control rods out of the reactor there will be an exponential rise of the neutron flux which can be written as follows:

$$\phi(t) = \phi_0 * e^{t/T}. \quad (13)$$

By measuring the detector count rate as a function of time it is possible to determine the reactor period τ_e by fitting the measured results to an exponential function. Next, the stable reactor period can be used to calculate the reactivity by using equation (14) or equation (15)[2]:

$$\rho = \frac{l}{l + \tau_e} + \frac{\tau_e}{l + \tau_e} * \sum_{i}^{G} \frac{\beta_{i,eff}}{1 + \lambda_i \tau_e} \tag{14}$$

$$\rho/\beta_{eff} = \sum_{i}^{G} \frac{a_{i,eff}}{1 + \lambda_i \tau_e}. \tag{15}$$

Equation (15) is a simplification of equation (14), which also calculates ρ in dollars, thus relative to β, the delayed neutron fraction. Note that the first term in equation (14) can be dropped since it is negligibly small if calculated with reasonable values for l and τ_e, for example $2*10^{-5}$ s, and 100 s respectively, for the VENUS-F reactor. If the same values are used to calculate the fraction before the summation, it can be decided to equal this fraction to 1.
The relative abundances of precursor groups $a_{i,eff}$ are calculated as the $\beta_{i,eff}$ with respect to β. Next, a summation was taken of all the precursor groups, which is indicated by the letter G.

4.2 The Rossi-alfa method

The Rossi-α method [4] is based on the phenomenon of measuring a time correlation between a neutron and each subsequent neutron within a time frame. This means, that in a short period of time after the measurement of a neutron, there is a greater probability that additional neutrons will be detected than later in time. This probability P_t can be described by a decreasing exponential function with the prompt neutron decay constant as a coefficient α, as shown in equation (16):

$$P_t = a + b * e^{-\alpha * t}. \tag{16}$$

The second term in the equation represents the probability of detecting neutrons of the same fission chain as the trigger neutron at t=0 and it is called the correlated term. The first term represents the probability to detect neutrons from other fission chains and it is called the uncorrelated term.

By measuring the coefficient α with the Rossi-alpha method and β_{eff} with the Cf source method, it is possible to calculate the mean neutron generation time Λ, by using equation (17) [3]. In case the measurements take place in a critical reactor, equation (17) can be simplified to equation (18):

$$\alpha \equiv \frac{\beta_{eff} - \rho}{\Lambda} \tag{17}$$

$$\alpha \approx \frac{\beta_{eff}}{\Lambda}. \tag{18}$$

5 MONTE CARLO METHOD

Monte Carlo is an algorithm that simulates a physical process repeatedly to calculate unknown parameters. Each time the starting conditions are randomly sampled from a distribution of realistic values. By repeating the procedure numerous times, it is possible to obtain a detailed simulation of the physical process where the results are represented in the form of a distribution curve. Applied to a reactor system, the life of a neutron from its initial emission until its death by absorption or escape from the system is simulated. During its lifetime the neutron will undergo various interactions and as result has different outcomes for every neutron simulated. To simulate these interactions, nuclear data, such as cross section data which gives the probability of a particular interaction between a neutron and a target, are used. The frequency and the outcomes of the interactions are randomly sampled and simulated according to the laws of particle physics [20].

The nuclear interaction data obtained by measurements and theoretical models are gathered into data libraries which are called evaluated nuclear data files.

The Monte Carlo Method is well-suited to solve reactor physics problems because of the linearity of neutron transport. Neutrons are born and will only interact with the medium surrounding it and not with each other. The simplicity of the process and the potential to produce very accurate results makes the Monte Carlo Method optimal to simulate the neutron transport process. Additionally, the linearity makes it suitable for parallel calculation which increases the efficiency of the calculation and decreases the computing time [20].

5.1 SERPENT

Serpent is a three-dimensional, continuous-energy neutron transport code based on the Monte Carlo Method and is intended for reactor physics calculations in particular at fuel assembly level. The working on its predecessor "Probabilistic Scattering Game" (PSG) started in 2004 at VTT. The reason for starting on the Serpent code was that the general-purpose codes available were not well suited for lattice physics applications. The calculations were very time consuming and the calculations of certain parameters such as the effective delayed neutron fraction were beyond the capability of simulation codes. One goal of Serpent was to show that the limitations can be solved by developing a dedicated Monte Carlo lattice physics code. This makes the continuous-energy Monte Carlo Method a potential option for spatial homogenization in the near future [20], [21].

Eventually, Serpent 1 was released after re-writing PSG twice to correct a methodological flaw. This resulted in much better statistical precision. In addition, it was decided to include the possibility to implement burn-up calculations. However, since Serpent 1 was developed in a short amount of time, the code only consisted of different solutions. This meant that pieces of codes were constantly being added on top of the existing source code, which made the structure rather complex. The solution was to re-write the entire source code again with the aim of extending the burn-up capabilities and future technologies, such as multi-core CPU's and massive parallelization, which lead to the creation of Serpent2 [20], [21].

5.1.1 Iterated Fission Probability

The continuous-energy Monte Carlo method is used to calculate the static equations of the neutron flux in a direct simulation. To reduce the large computing time, the adjoint neutron flux is used as weighting function to calculate changes in the multiplication factor k_{eff}. This is important since the adjoint flux $\phi^*(\mathbf{r}, E, \mathbf{\Omega})$ is proportional to the reactivity of a reaction induced by a neutron in position r with energy E and direction Ω. However, calculating the adjoint neutron flux $\phi^*(\mathbf{r}, E, \mathbf{\Omega})$, which is the eigenfunction of the static adjoint equation, is difficult with the Monte Carlo method. Furthermore, kinetic parameters, such as the delayed neutron fraction β_{eff} and the neutron generation time Λ, are estimated using the adjoint flux. Thus, as alternative method based on the continuous-energy Monte Carlo method, the iterated fission probability method is used. It has been shown in [22] that the iterated fission probability I_{FP} is proportional to the adjoint flux, which makes it possible to calculate β_{eff} and Λ without the need to estimate ϕ^* [22].

The iterated fission probability I_{FP} is the asymptotic power which originates from a neutron in spatial position $\theta = (\mathbf{r}, E, \mathbf{\Omega})$. This neutron will stochastically induce a fission reaction which yields neutrons, also called progenies, in the next generation. The progenies from the neutron induce a chain reaction in the reactor core and produce new progenies in the following generations. As the number of generations λ increases, distributions of the neutron flux $\phi^{(\lambda)}$ and the fission neutron emission produced by the progenies converge to a fundamental mode. The convergence to a fundamental mode is reached in generation L and thus the reactor power, in generation λ reaches a definite level. The reactor power (also called the 'asymptotic' power) refers to the fact that a sufficiently long time between the initiating event and generation L has been passed [23]. The balance equation of the reactor power can be expressed with a multiplication of $1/k_{eff,}$ which is also the eigenvalue of the static neutron transport equations without any outer source. This makes that the iterated fission probability $I_{FP}(\theta)$ is proportional to the adjoint flux $\phi^*(\theta)$ [22].

Using I_{FP} it is possible to calculate $\beta_{eff}^{(\lambda)}$ as the number of descendant fission neutrons in generation $L_0 + 1 + \lambda$ originating in delayed neutrons in generation $L_0 + 1$ on the total number of fission neutrons in generation $L_0 + 1 + \lambda$. Furthermore, $\Lambda^{(\lambda)}$ can be calculated by storing the life time and information on the progenies for the source in generation $L_0 + 1$.

6 METHODS AND MATERIALS

6.1 CORE COMPOSITION AND DETECTOR POSITIONS

The measurements described in this thesis were performed at the CC12 configuration of the VENUS-F reactor. Figure 11 gives a radial view of the reactor core CC12 with the positions of the applied detectors used indicated.

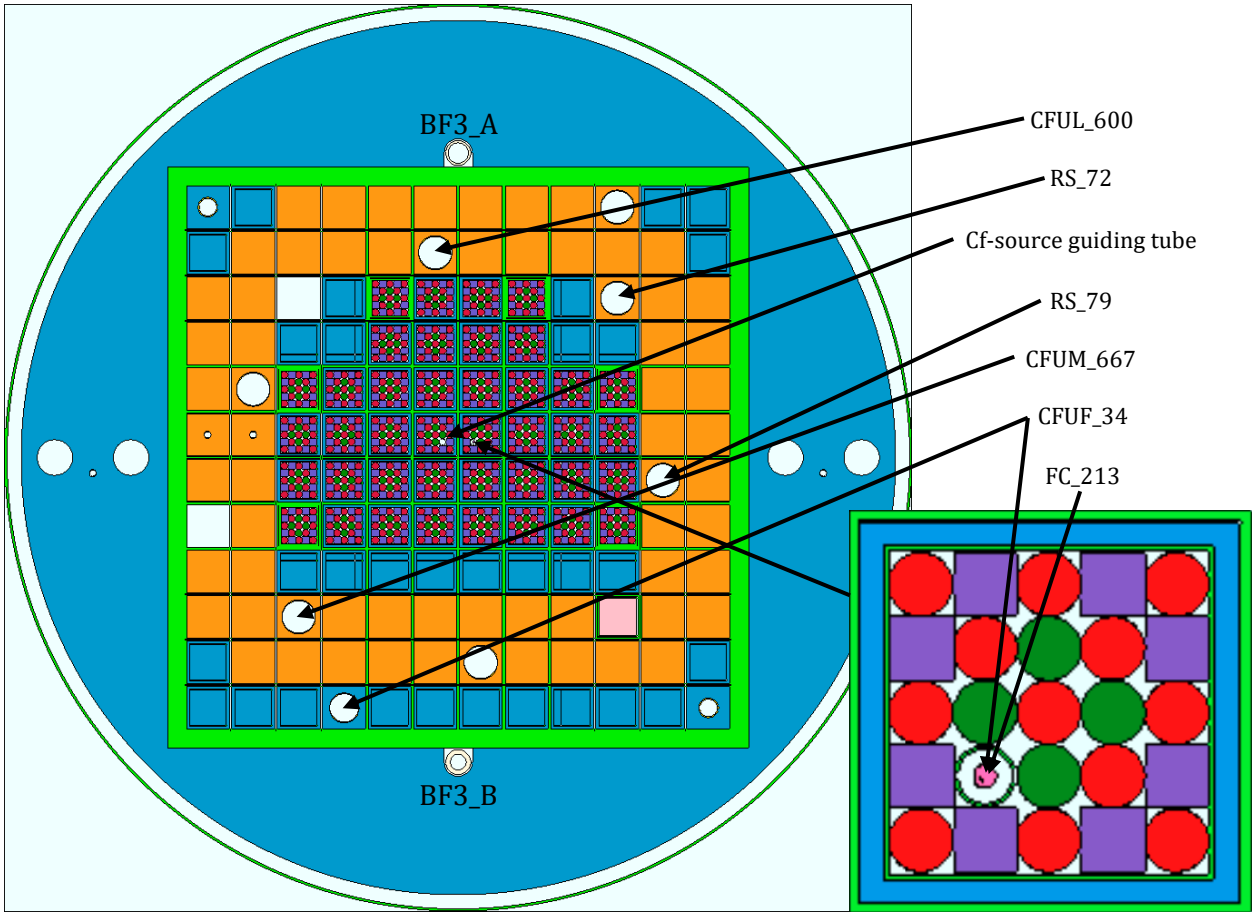

Figure 11: Radial view of CC12 with the positions of the detectors indicated. Detector CFUF_34 was used for measurements in two different positions (in the fuel zone and in the lead reflector).

As can be seen in the right part of Figure 11, a miniature fission chamber detector such as CFUF_34 or FC_213 can be inserted in the guiding tube in the experimental fuel assembly EFA1. Both detectors have a layer of ^{235}U with a mass of 1 mg. As listed in Table 2 detector CFUF_34 is used for the calibration of the control rods and also for axial measurements where the detector is moved axially from the bottom reflector to the top reflector. Detector FC_213 is only used for the measurement of the change in fission rate (Q_f see equation (12)), while the Cf-source is inserted into the reactor via a guiding tube located in EFA2. The experimental fuel assembly EFA2 is the mirror image of EFA1 (see Figure 11), where the guiding tube is positioned at the bottom right. The position of this assembly is indicated as position (-1, 1). Besides CFUF_34, detector CFUM_667 is used to measure the count rate during the calibration of the control rods. This detector has a deposit mass of 10 mg, which is 10× bigger than in case of CFUF_34.

To measure the correlated counts for the Rossi-α experiment, detectors CFUL_600, RS_72 and RS_79 are used. This is due to their high deposit mass of respectively 1000 mg for CFUL_600 and 100 mg for a RS detector. The high deposit mass ensures a high count rate. Lastly, detectors BF3_A and BF3_B are used for the axial measurements where the Cf-source is moved from the bottom reflector to the top reflector. These two detectors are positioned in the radial reflector and are proportional counters.

Table 2: Name of the detectors used with their respective position in CC12, deposit mass ^{235}U and there dead-time.

Detector name	**CFUF_34**	**CFUM_667**	**FC_213**	**CFUL_600**	**RS_72**	**RS_79**	**BF3_A**	**BF3_B**
Position	(-3, -6) (1, 1)	(-4, -4)	(1, 1)	(-1, 5)	(4, 4)	(5, -1)	Outer reflector	
Deposit mass (mg)	1	10	3	1000	100	100		
Dead-time (ns)	90	123		130	160	160		
Experiment	CR cal. Axial FC	CR cal., monitor	Q_f	Rossi-α			Axial Cf	

Figure 12 gives a view of a type of ^{235}U fission chambers that are used to detect neutrons. It has a shape of a cylindrical tube which is connected through a single cable with the high voltage, pre-amplifier and the amplifier.

Figure 12: Example of a ^{235}U CFUL fission chamber used in this thesis (from the Photonis catalogue) [24].

In case of the FC_213 detector, the pre-amplifier is placed inside the bunker, where the reactor core is positioned, and all other electronic units are placed outside. In case of the other fission chambers, the electronic units are placed in the control room. The high voltage source is set to supply the fission chamber with a voltage in a range of 300 V to 700 V and the signal is processed in a programmable high speed pulse amplifier (PHSPA) [27]. The data acquisition system used for the measurements with the FC_213 detector is the GENIE-2000 software [25], the signals from the other fission chambers are recorded with a LabVIEW-based in-house software.

6.2 MEASUREMENT OF THE EFFECTIVE DELAYED NEUTRON FRACTION

As introduced in section 4.1, the californium-source method is used to determine the delayed neutron fraction β_{eff} as described in equation (12), which is repeated here:

$$\beta_{eff} = \frac{S_{Cf}}{|\rho_{\$}| * Q_f * \bar{\nu}} * \frac{1}{f} * \frac{F^{+}_{\chi,Cf}(0)}{\overline{F^{+}_{\chi}}}.$$

The parameters in the equation can be classified according to their determination method: i.e. calibration data, measurement and calculation. In this thesis, the following methods were used.

The strength of the source S_{Cf} is determined using its certificate which provides the activity or strength at the calibration date. The subcriticality $\rho_{\$}$ of the VENUS-F core is measured with calibrated control rods. The calibration is performed using the positive period method combined with the compensation method. Then the calibrated control rods are used to measure the reactivity of three sub-criticality states. Next, the change in fission rate Q_f, due to inserting the californium source in the reactor core, is determined. However, the change in fission rate is only measured in one point in the reactor and the source neutrons will not change the fission rate equally everywhere in the reactor core. The importance of a neutron is represented by the adjoint flux: a neutron in position **r** with energy E and direction **Ω** will not always have the same effect on the multiplication system. Therefore, corrections have to be made for the experimental determination of the change in fission rate in a single point to the change in fission rate in the whole reactor.

The first correction factor is *f*, which represents the conversion factor for the change in fission rate from one point to the whole reactor. The second correction factor $F^{+}_{\chi,Cf}(0)/\overline{F^{+}_{\chi}}$ represents the importance of a source neutron to the multiplication factor for the whole reactor core. Both correction factors are calculated through simulation with Serpent2. Besides these parameters, the delayed neutron parameters and the average number of neutrons emitted per fission $\bar{\nu}$ are also calculated with Serpent2.

6.2.1 Calibration of the control rods

To calibrate the control rods, it is important to start with a critical position. In this position both control rods have the same height, and the reactor core is critical. This means that the multiplication factor k_{eff} is equal to one and that the reactor period is infinite. Then, in the case of the VENUS-F core where there are two control rods, the first control rod CR1 is pulled up. By pulling CR1 out of the core, there will be an insertion of a positive reactivity. The reactor will become supercritical and the multiplication system rises exponentially. In the control room it is possible to estimate the reactor period or the time needed for the neutron density to change by a factor e = 2.718. Subsequently, the count rate is measured for two or three time this estimated reactor period.

After the reactor period measurement, the second control rod CR2 is inserted until criticality is reached and thus the supercriticality is compensated. Next, the first step is repeated until CR1 is completely pulled out of the reactor core. Lastly, the same process is repeated by pulling CR2 after returning to the critical position.

At the start it is decided at what reactor power the measurements will take place. It is the best to choose a reactor power where the neutron flux at the detector locations is such that the detector count rate is high enough to reach sufficient number of measured counts and at the same time not too high to prevent saturation of the detectors and keep the dead time low. In the case of this experiment detectors CFUF_34 and CFUM_667 are used. In Table 2 the dead time for both detectors is listed and for which the measured count rate must be corrected. Then, counts per second can be fitted as a function of the time to determine the reactor period. Next, the inserted reactivity according to the insertion or removal of the control rod can be calculated with equation (15).

6.2.2 Measurement of the change in fission rate

The change in fission rate is measured with detector FC_213 in position (1,1) while the californium source is in position at (-1,1). The detector is firstly connected with a pre-amplifier because the signal is only around 20 μA. Next, the signal arrives in the control room where it is amplified to ~1 V before it is analysed with a multipurpose analyser and data-acquisition system. The signal reaches a computer with the GENIE-2000 spectroscopy software.

The count rate measured with the FC_213 is small (less than 10 counts per second), thus no corrections for dead-time have to be made. The change in fission rate is determined for three subcriticality levels. The reactivity is determined thanks to the control rods calibrated as described in section 6.2.1. For every subcriticality level, the background count rate (without the presence of the Cf-source) is measured. Afterwards, the average change in fission rate is calculated for a critical core through correction of the three subcriticality levels.

6.2.3 Calculations with Serpent2

To simulate the CC12 reactor core in Serpent2 a basis is provided in the form of the code for a previous core composition (CC5). This code is adapted to fit the current core composition. Firstly, a critical core composition is simulated to calculate parameters such as k_{eff}, $\bar{\nu}$, β_{eff} and also the relative abundance of the precursor groups $a_{i,eff}$ with their respective decay constants λ_i. Then, the k_{eff} for the three subcriticality positions is calculated. For the three subcriticality positions new calculations where the external californium source is present are made to determine the factors f and $F^{+}_{\chi,Cf}(0)/\overline{F^{+}_{\chi}}$ in equation (12).

To verify if the calculated correction factors are reliable and representative for the whole reactor core extra experiments are performed. These experiments are axial dependent measurements when the californium source or the detector is moving from the bottom reflector to the top reflector.

When moving the californium source axially trough the reactor it is possible to determine the contribution of a californium source neutron in the reactor core. When the source and thus a neutron is positioned near the bottom or top reflector, there will be less effect on the multiplication system of the reactor. The change in fission rate is less outspoken. This axial measurement is performed to verify the calculation of the neutron importance factor or adjoint flux. For the measurements two detectors in positions A and B in the radial reflector are used, see Figure 11. Both detectors BF3_A and BF3_B are proportional counters. The results are directly visible in the control room.

When the detector is moved axially, it is possible to determine the spatial distribution of the fission rate in the reactor core. The fission rate is measured with detector CFUF_34. Since the reactor power is not constant throughout the whole measurement a monitor detector CFUM_667 is used to normalize the count rate. The monitor detector is positioned as shown in Figure 11 far from the CFUF_34 detector and thus is the influence of the movement of the detector on the monitor count rate negligible.

6.3 MEASUREMENT OF THE MEAN NEUTRON GENERATION TIME

The determination of the mean neutron generation time Λ is based on equation (17) introduced in section 4.2 and repeated here:

$$\alpha \equiv \frac{\beta_{eff} - \rho}{\Lambda}.$$

The prompt neutron decay constant α is experimentally determined using the Rossi-α method when the correlated counts in a time window are measured. To receive statistically accurate data, it is important to measure long enough to get a high enough amount of counts in each time bin. The resulting data can be fitted with an exponential which will ensure the determination of α. The measurements can take place in the critical reactor as well as subcritical, which results in the different values of α. The correction for the reactivity in equation (17) should lead to the same value of the mean neutron generation time.

The detectors used to execute the neutron noise technique are CFUL_600, RS_72 and RS_79. All three detectors have a high deposit mass of respectively 1000 mg for CFUL and 100 mg for RS. The high deposit mass is needed to ensure a sufficiently high count rate. The signals from the detectors are transmitted to PHSPA to be further assimilated and processed.

7 RESULTS

7.1 DETERMINATION OF THE EFFECTIVE DELAYED NEUTRON FRACTION

7.1.1 Determination of the californium source strength

Initially a ^{252}Cf source available at the VENUS-F laboratory containing 1.5 µg ^{252}Cf was planned to be used. The source is spread over an active spot with a diameter of 4 mm, surrounded by a stainless-steel truncated cone with a base of 10 mm diameter [26]. The ^{252}Cf source had an activity of 28.9 ± 0.78 MBq on April 21st, 2004. The activity was calculated using following equation (13), where the half live of ^{252}Cf is 2.645 years with an uncertainty of 0.008 years [27], [28]:

$$A_t = A_0 * e^{(\frac{-\ln(2)}{T_{\frac{1}{2}}} * t)}. \quad (13)$$

In annex A1, Figure 21 shows the activity of the source in the year it was calibrated until the year in which the measurements took place. The strength of the first ^{252}Cf source can be calculated based on next formula (14):

$$S_{Cf} = Abundance * \bar{\nu}(^{252}\text{Cf}) * A_t. \quad (14)$$

Where the abundance of ^{252}Cf is 3.092% and the number of neutrons released during one fission is 3.7676 [5], [28].Figure 22 in annex A1 shows that the strength of the source decreases in time and gives the strength of the ^{252}Cf source during the academic year of the measurements.

A stronger ^{252}Cf source became available shortly before the experiments and it was decided to use that source containing 200 µg ^{252}Cf for which the strength was calibrated on October 16th 1993. The initial strength of the second ^{252}Cf source was $4.97*10^8$ n/s (with 1.5 % uncertainty) and decreased exponentially over time as shown in Figure 23 in annex A1 shows. Furthermore, Figure 24 in annex A1 shows the strength of ^{252}Cf source 2 during the academic year of the measurements.

7.1.2 Calibration of the control rods

As is explained in section 6.2.1 the first step is to calibrate the control rods. This is done by using the compensation method and the positive period method. Firstly, the critical high is determined and set at 428.4 mm for both control rods CR1 and CR2. Then, Table 3 show that CR1 and CR2 are both gradually pulled out of the reactor in steps of approximately 50 mm. Every time the reactor is supercritical the count rate is measured with detectors CFUF_34 and CFUM_667 and the data are recorded with the time bin of 1 s. Figure 25 to Figure 36 in annex A2 show the fission chamber count rates after every movement of the control rods. The data is fitted to an exponential which allows the calculation of the reactor period. However, since both detectors have a dead-time, the count rates need to be corrected for that. Figure 37 and Figure 38 in annex A2 give the percentual correction for both detectors.

Table 3: Measured reactor period and reactivity for every position of the control rods during calibration using the compensation method.

	CR1(mm)	CR2(mm)	τ_e (s)	ρ (pcm)	CR1 (pcm/mm)	CR2 (pcm/mm)
Critical	428.3	428.3	∞			
T1	500.0	428.3	151.4	47.7	0.67	1.45
	500.0	395.5	∞			
T2	550.0	395.5	302.1	26.1	0.52	1.50
	550.0	378.1	∞			
T3	600.0	378.1	424.7	19.1	0.38	1.53
	600.0	365.6	∞			
Critical	428.3	428.3	∞			
T4	428.3	500	66.6	90.8	0.79	1.27
	313.4	500	∞			
T5	313.4	550	144.5	49.6	0.79	0.99
	250.6	550	∞			
T6	250.6	600	207.5	36.4	0.72	0.73
	200.2	600	∞			

The reactor period values determined using equation (13) are shown in the third column of Table 3. Next, the delayed neutron parameters were calculated with Serpent2 using the JENDL-4.0 nuclear data library, see Table 8. These values were used in equation (15) for every reactor period to determine the reactivity of each supercritical state, which is indicated in the fifth column of Table 3. Furthermore, dividing the reactivity of T1 to T3 by the difference in positions of CR1 between the critical and supercritical core gives the differential reactivity insertion by distance of the control rod. This also applies for reactor periods T4 to T6 and the movement of CR2. Eventually, Figure 13 can be constructed as the differential curves for CR1 and CR2 in function of their position in the reactor core.

Besides the differential curve, the integrated curve is also determined. At position 600 mm the control rods are completely pulled out of the reactor core. With every mm CR1 and CR2 are inserted into the reactor core, a negative reactivity is inserted as is shown in Figure 14.

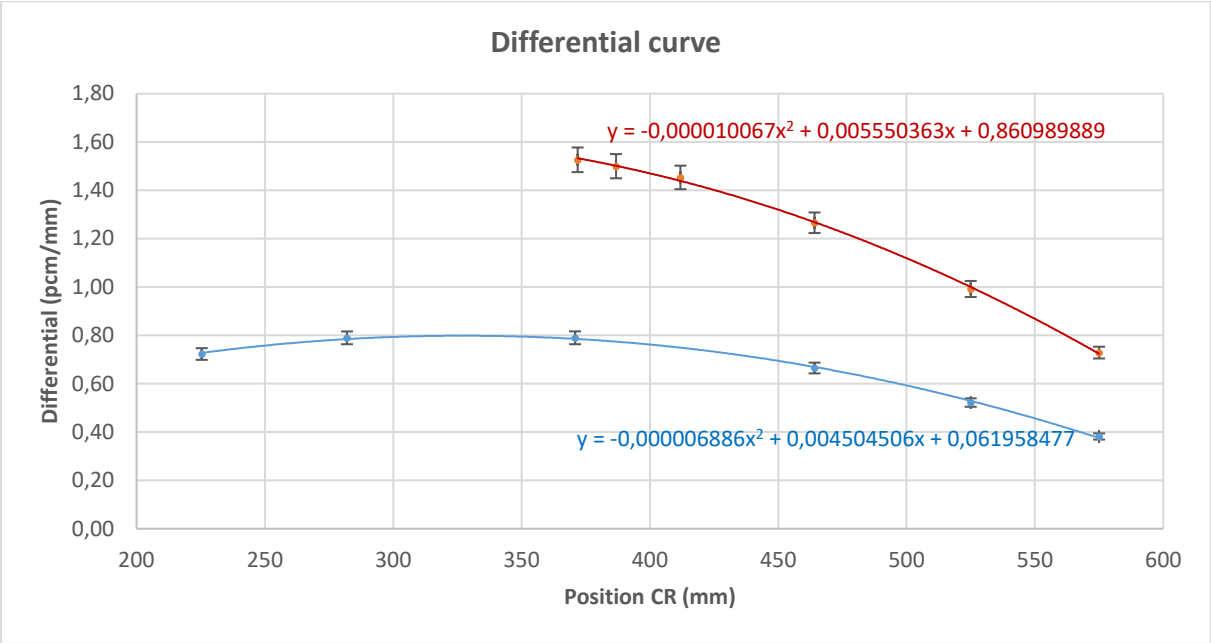

Figure 13: Differential curve of CR1 (blue) and CR2 (red).

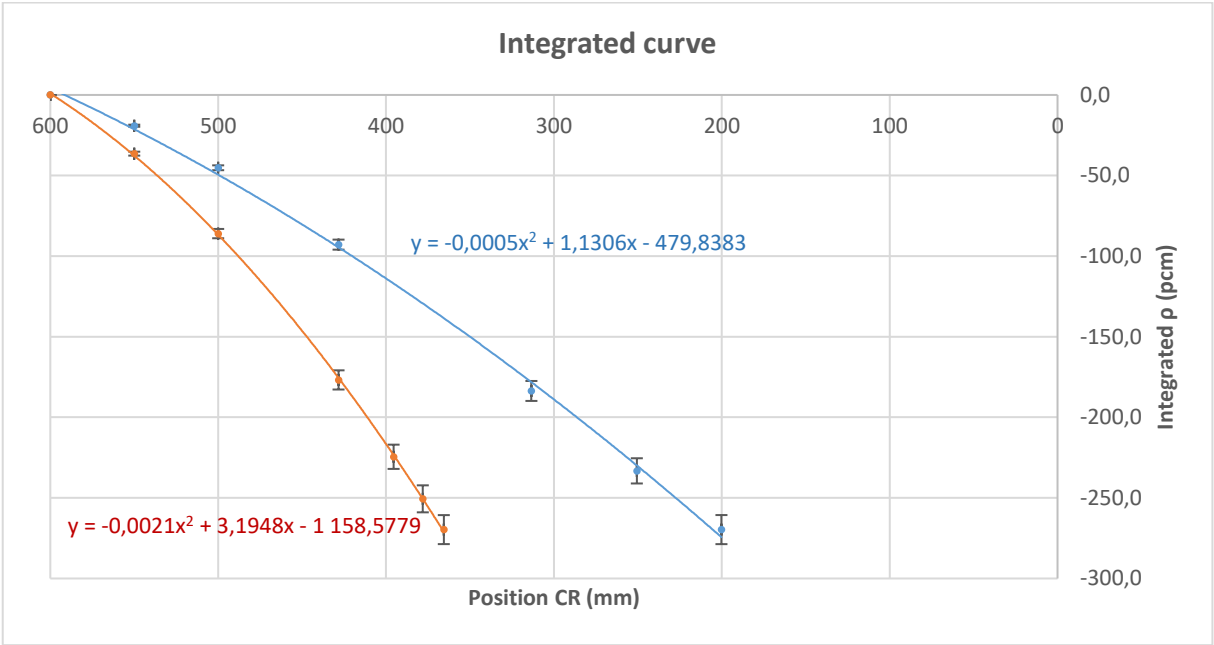

Figure 14: Integral curve of CR1 (blue) and CR2 (red). At position 600 mm a control rod is fully pulled out of the VENUS-F core.

In both Figure 13 and Figure 14 the absolute uncertainty is indicated. The absolute uncertainty can be calculated from the relative uncertainty which consists of different aspects as is indicated in Table 4.

The uncertainty is calculated through error propagation. First, the uncertainty on the exponential fit according to equation (13) in MS Excel for both detectors is determined. This is done by eliminating one third of the data and calculating the relative difference in the determined reactor periods. Next, a weighted average of the uncertainty of the fit for both detectors is calculated. Through the weighted average of the detectors and the decay constant the uncertainty on the denominator of equation (15) can be calculated. Together with the uncertainty of the abundance of

the precursor groups (numerator of equation (15)) this gives the uncertainty on the calculation. Table 4 shows that the uncertainty on the reactor periods are 0.14%-0.15%. Thus, the total uncertainty on the reactivity is mostly given by the uncertainty from the nuclear libraries, which is set at 2.5%.

Table 4: Uncertainty on the calculated reactivity corresponding to the respective reactor period and the error propagation.

Uncert ρ	Total	Nuc. library	Period	Abundance	Denominator	Weight av.	Fit of CFUF	Fit of CFUM
T1	2.65%	2.50%	0.15%	0.307%	0.35%	0.71%	0.82%	0.64%
T2	2.65%	2.50%	0.15%	0.118%	0.07%	0.14%	0.12%	0.24%
T3	2.65%	2.50%	0.15%	0.122%	0.05%	0.10%	0.17%	0.08%
T4	2.64%	2.50%	0.14%	0.084%	0.29%	0.59%	0.62%	0.57%
T5	2.64%	2.50%	0.14%	0.14%	0.23%	0.48%	0.64%	0.41%
T6	2.65%	2.50%	0.15%	0.243%	0.11%	0.23%	0.35%	0.19%

7.1.3 Measurement of the change in fission rate

The next step is to measure the change in fission rate when the californium source is inserted in the reactor core. The FC_213 detector was placed at a radial distance of 56 mm from the Cf-source (Figure 11). An example of a spectrum of fission fragments obtained after measuring the count rate for approximately 1 hour at a certain subcriticality level is shown in Figure 15. It has been decided to use three different subcriticality levels. The three subcriticality levels depend on the position of CR1 which is set at 300 mm, 250 mm and 200mm, which gives a reactivity of -13.71, -19.03 and -23.96 cents, respectively. Figure 39 to Figure 44 in Annex A3 give the measured spectra for the three subcriticality levels and also the background spectra for when the californium source is not inserted.

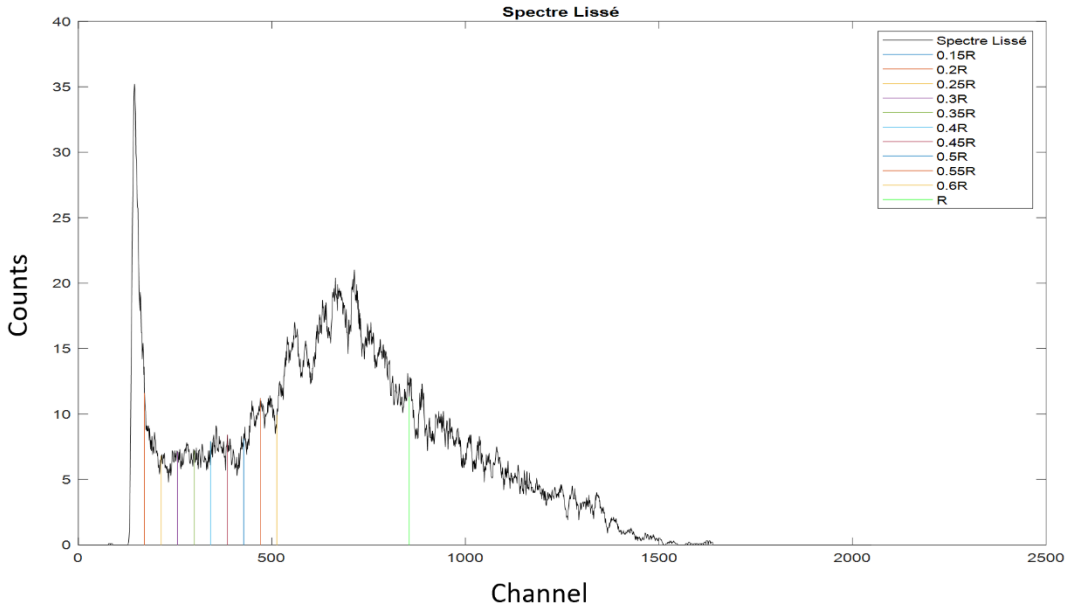

Figure 15: Spectrum of fission fragments measured with FC_213. Different discrimination levels correspond with a calibrated effective mass of ^{235}U present in the detector deposit. The counts per channel is plotted in function of the channel.

As can be seen in Figure 15 and Table 5, there are different discrimination levels which correspond to a calibrated effective mass of ^{235}U present in the detector deposit. First, for every CR1 position the background is subtracted from the measured count rate for every discrimination level. The count rate per mass deposit is determined by dividing the count rate by the effective mass. Ideally the ratio of the count rate and the effective mass has to be equal for every discrimination level since the count rate is calibrated according to its effective mass. Thus, an average can be calculated over the discrimination levels. However, perturbations can occur in the first discrimination levels due to electronic noise. Furthermore, higher discrimination levels have a low number of counts resulting in a higher statistical uncertainty. This is why only the middle discrimination levels are used to calculate the average. The used count rates are indicated in Table 5 and the average for the subcriticality levels is displayed in Table 6 together with the standard deviation on the counts, which is smaller than 1 %. The count rate per mass deposit is normalized by multiplying by the subcriticality in dollars. The average change in fission rate caused by inserting the californium source is 247.3 $×cps/g.

Table 5: Measured count rates on different subcriticality levels, calibrated according to the discrimination levels and their effective mass. Corrected for the background. The underlined values are used to calculate the average value that is then presented in Table 6.

R	Meff (µg)	Count rate pos 1	Count rate pos 2	Count rate pos 3	cps/g	cps/g	cps/g
0.15R	3023	5.41	3.91	3.13	1790.91	1294.09	1034.17
0.2R	2964	5.02	3.53	2.79	1693.96	1190.71	941.66
0.25R	2902	5.20	3.66	2.91	*1793.09*	1259.94	1001.71
0.3R	2837	5.10	3.66	2.92	*1797.24*	*1288.58*	*1030.50*
0.35R	2765	4.95	3.58	2.86	*1791.86*	*1295.88*	*1035.69*
0.4R	2685	4.81	3.50	2.80	*1791.24*	*1302.55*	*1042.22*
0.45R	2593	4.65	3.39	2.72	*1794.00*	*1306.16*	*1049.25*
0.5R	2483	4.51	3.27	2.63	1815.62	1315.85	1058.16
0.55R	2346	4.31	3.11	2.52	1838.88	1325.12	1074.99
0.6R	2187	4.10	2.92	2.40	1873.42	1333.50	1095.35

Table 6: Average count rate per gram of the deposit mass normalized for the subcriticality.

ρ (cents)	-13.71	-19.03	-23.96
Av. cps/g	1793.48	1298.29	1039.41
Stv	2.36	7.75	8.12
Rel. Stv (%)	0.13	0.60	0.78
Norm Av. $/(s×g)	245.9	247.0	249.0

7.1.4 Calculations by Serpent

As stated in section 6.2.3 the reactor core CC12 is simulated in Serpent2. The calculations are performed using the Newton calculation cluster at SCK CEN. Newton is the HPC (High-performance computing) cluster with the core operating system CentOS 7.x. It consists of several thousand of computing cores. The test Serpent2 calculations when the reactor geometry was being created are performed as serial jobs on single CPU. The production Serpent2 calculations (results shown in this section) are performed with 72 CPUs in parallel.

Firstly, the critical core is simulated by setting CR1 and CR2 at a position of 428.3 mm. This gives the parameters presented in Table 7. Next, parameters such as the reactivity and the prompt neutron decay constant α can be calculated with the given parameters. The simulation of the critical core gives a k_{eff} of 0.9994 making the simulation fairly accurate with only a difference of 0.0006 from a real critical core. Thus, the simulated core only differs from criticality with a reactivity of -57 pcm.

Table 7: Results and relative uncertainty obtained by simulating reactor core CC12 in Serpent2 by positioning CR1 and CR2 @428.3mm. The absolute uncertainty is calculated with the relative uncertainty given by Serpent2.

	Value	Abs. Uncert	Rel. Uncert (%)
$\mathbf{k_{eff}}$	0.9994	2.50E-05	0.0025
ρ (pcm)	-57	2.50	
$\overline{\nu}$	2.5117	0.40E-05	0.00016
Λ (ns)	1961	2.61	0.133
$\mathbf{\beta_{eff}}$ **(pcm)**	748	0.39	0.052
α (1/s)	3814	5.45	

Serpent2 also provides the relative abundancy of the precursor groups, their relative uncertainty and the decay constant of the precursor groups. The nuclear data library JENDL-4.0 is used which contains six precursor groups, as indicated in Table 8. As stated in section 4.1.1, the abundancy is calculated with respect to the delayed neutron fraction β_{eff}, which is calculated to be 748 pcm.

Table 8: Relative abundance of precursor groups, their uncertainty and the decay constants of every precursor group calculated with Serpent2 based on JENDL-4.0 library.

Precursor	1	2	3	4	5	6	
Total β_{eff} (pcm)							748
$a_{i.eff}$	0.0298	0.1986	0.1948	0.3881	0.1436	0.0451	1.00
Rel. Uncert. (%)	0.307	0.118	0.122	0.084	0.139	0.243	
λ_i	0.01252	0.03077	0.11669	0.31413	1.23535	3.38531	

Lastly, axial measurements are performed to support Serpent2 calculations of parameters *f* and $F^{+}_{\chi.\ Cf}(0)/\overline{F^{+}_{\chi}}$ in equation (12). First, the Cf-source is moved axially through the reactor core while measuring the fission rate at positions A and B (see Figure 11). This measurement is performed in the first subcritical level (namely with a reactivity of -13.71 cents). Next measurements are performed where the fission chamber is moved axially through the critical reactor. Sections 7.1.4.1 and 7.1.4.2 discuss the calculated results with the results obtained with the axial measurements.

7.1.4.1 Verification by axial measurement with the moving Cf-source

To complete the determination of β_{eff}, the parameters *f* and $F^{+}_{\chi.\ Cf}(0)/\overline{F^{+}_{\chi}}$ from equation (12) need to be determined with Serpent2. However, the new version of the Serpent2 code that is planned to contain direct calculation of the adjoint flux has not been released yet. An alternative combination of measurements and calculations is applied to determine $F^{+}_{\chi.\ Cf}(0)/\overline{F^{+}_{\chi}}$. The detector count rate is measured while moving the californium source axially through the reactor core, see Figure 16. The count rate is normalized to the maximum in the middle of the active fuel part.

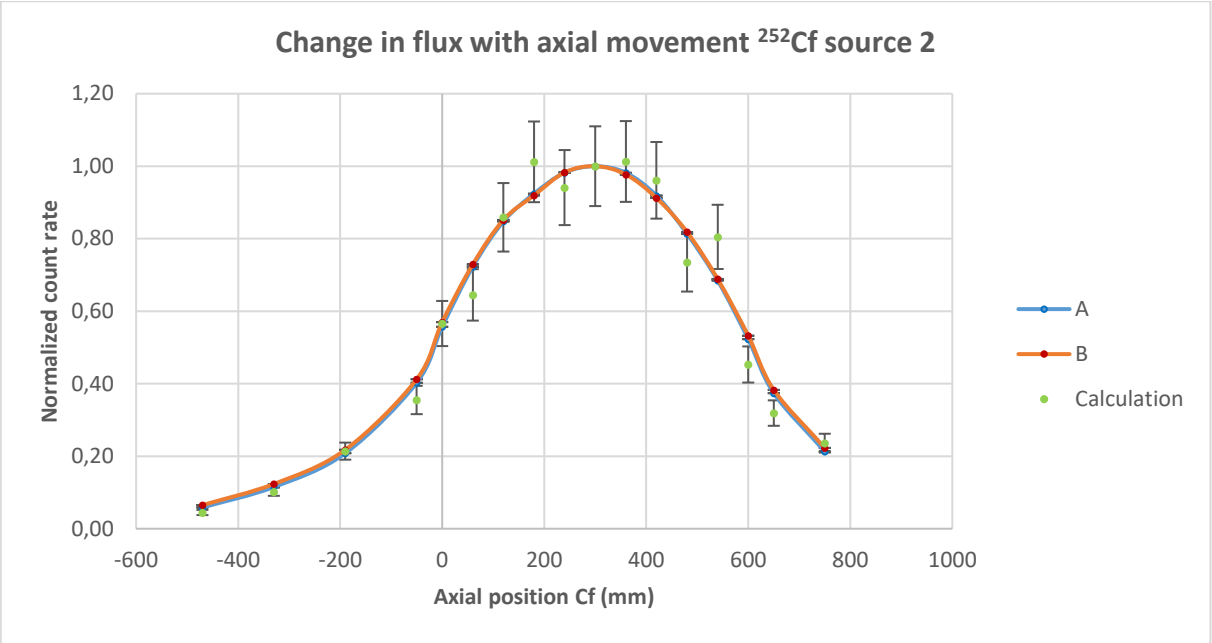

Figure 16: Normalized count rate as a function of the axial position of ^{252}Cf source 2 measured at reactivity of -13.71 cents with proportional counters BF3_A and BF3_B compared with calculations.

Table 14 in annex A4 gives the measured count rate of the two detectors. To have a statistically accurate value an average is taken over five values for each detector which is then normalized to one in the middle plane of the core. The uncertainty is calculated by taking the inverse of the square root of the counts for every position of the californium source. As can be seen in Figure 16 and Table 14 both normalized measured count rates give approximately the same value or curve shape.

The results from the axial calculations follow the general trend set by the measured count rates. The results and the absolute uncertainty of the normalized calculations are also shown in Figure 16 and Table 15. The relative difference with the measured and normalized response of detector BF3_B is shown in Table 15. As can be seen the statistical uncertainties of the calculated detector count rates are big (around 10%) because the detectors are located in the outer reflector.

To determine the $\overline{F_\chi^+}$ term, the integral under the curve in the fuel zone part plotted in Figure 16 needs to be determined. The distribution is fitted with a polynomial function (Figure 17) that is then integrated. Using the integrated function, the value of the $\overline{F_\chi^+}$ term is determined. As the distribution is normalized, the central term $F_{\chi.\ cf}^+(0)$ equals 1. The entire parameter $F_{\chi.\ cf}^+(0)/\overline{F_\chi^+}$ is then equal to the reciprocal of the $\overline{F_\chi^+}$ term, see Table 9.

Table 9: Integral of the axial distribution through the fuel zone when moving the Cf source at reactivity of -13.71 cents.

	Normalized A	**Normalized B**	**Calculation**
$\overline{F_\chi^+}$	506.8	507.7	510.2
$\overline{F_\chi^+}$ / mm	0.845	0.846	0.850
$F_{\chi.\ cf}^+(0)$	1.00	1.00	1.00
$F_{\chi.\ cf}^+(0)/\overline{F_\chi^+}$	1.184	1.182	1.176

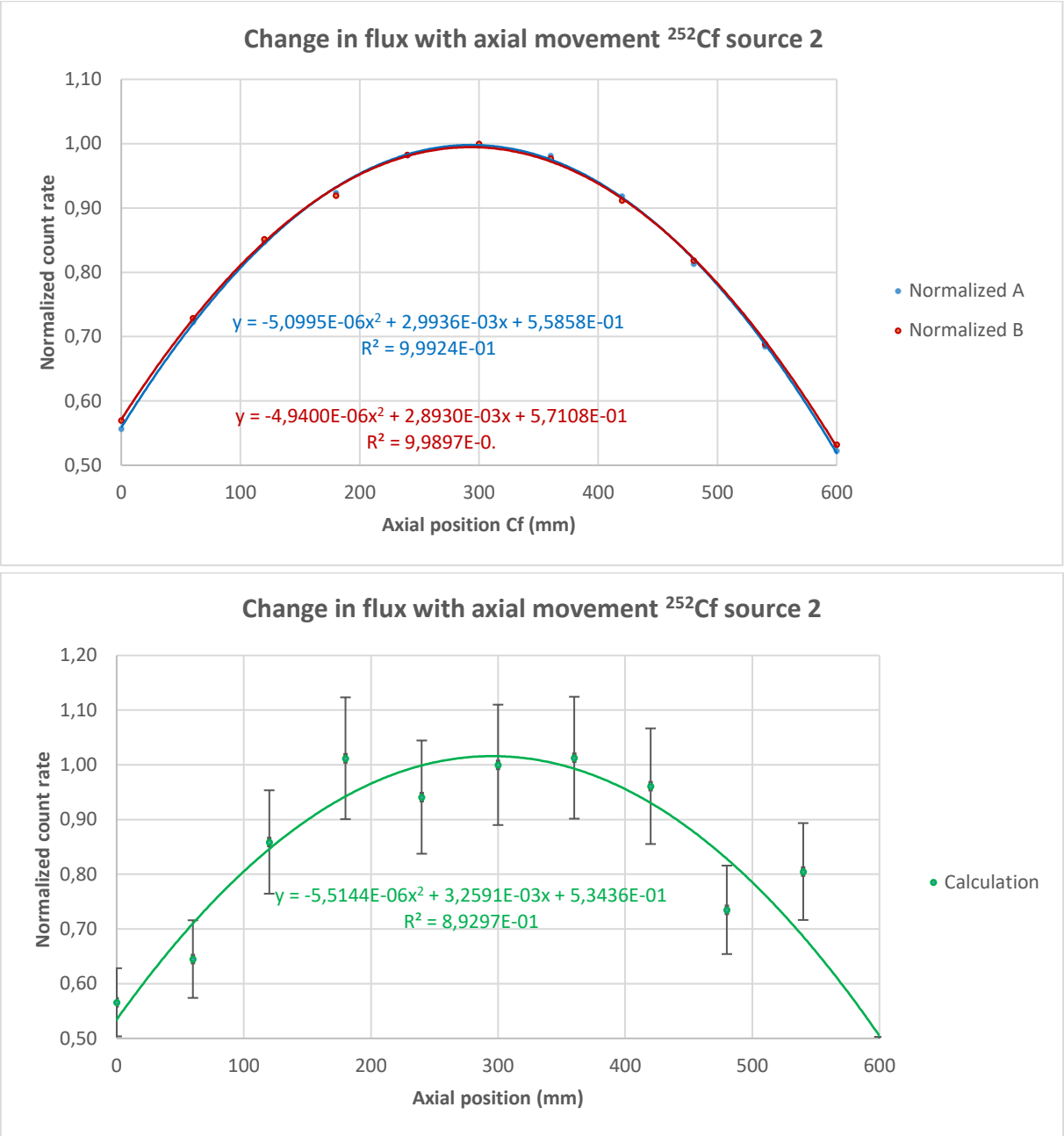

Figure 17: Fits of normalized count rate as a function of the axial position of ²⁵²Cf source 2. Top: measurements, bottom: calculation.

In principal, the value of the parameter $F^{+}_{\chi.\ Cf}(0)/\overline{F^{+}_{\chi}}$ depends on the reactivity. Calculations with moving Cf source are performed for each of the three subcriticality levels. However, as can be seen in Figure 18, the calculated distributions agree with each other within the uncertainties. Due to time constraints, it was not possible to reach smaller uncertainties of the calculations. Therefore, the same average value of $F^{+}_{\chi.\ Cf}(0)/\overline{F^{+}_{\chi}} = 1.183$ for the measurement with two detectors from Table 9 is used for all the three subcriticality levels.

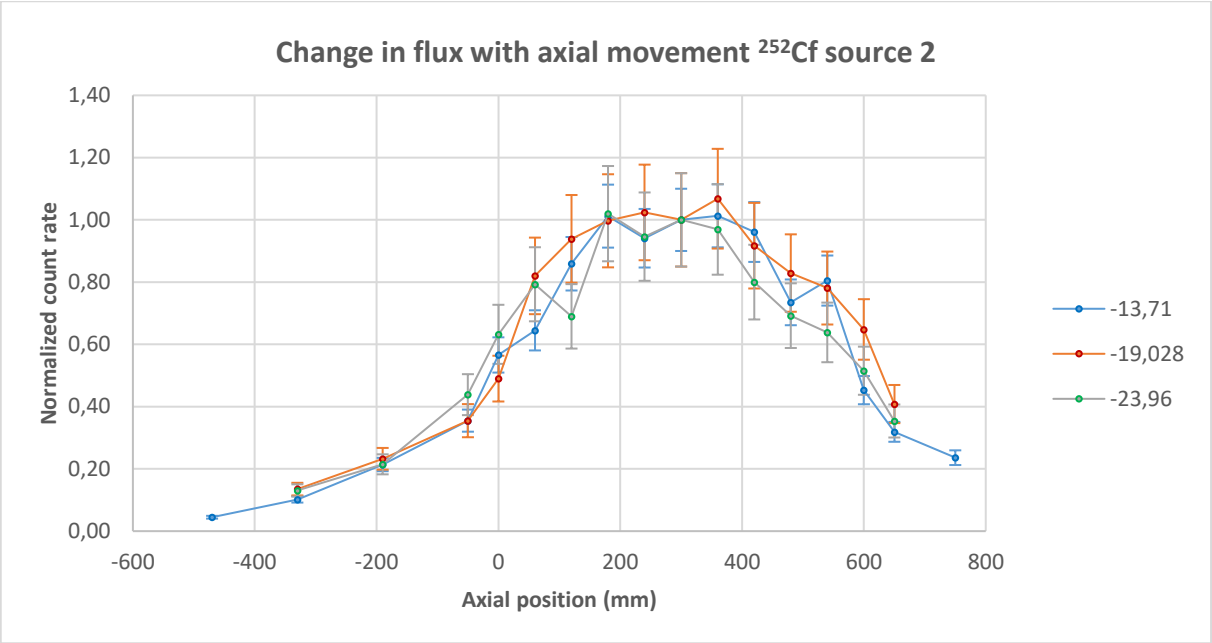

Figure 18: Normalized count rate as a function of the radial position of ²⁵²Cf source 2 calculated at three reactivity levels.

The method requires to determine the adjoint flux in the entire core volume, therefore, additional simulations are made to calculate radial distribution in a similar way as it was done for the axial distribution. The Cf source in the Serpent2 geometry is placed at several radial positions (always in the middle plane of the core) and the detector count rates are again calculated, see Figure 19. Through fitting and integration, the value of parameter $F^{+}_{\chi.\ cf}(0)/\overline{F^{+}_{\chi}}$ obtained in this way is 1.183, which very well agrees with the value obtained when analyzing the axial distribution.

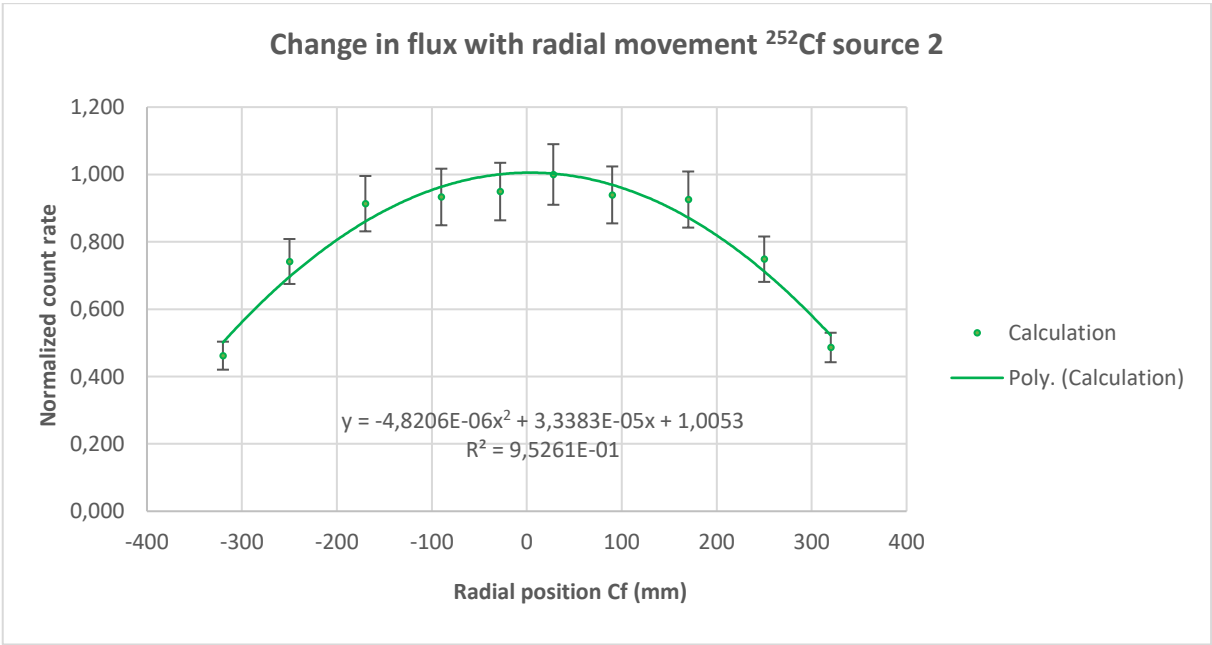

Figure 19: Normalized count rate as a function of the radial position of ²⁵²Cf source 2 calculated at reactivity of -13.71 cents.

7.1.4.2 *Verification by axial measurement with a moving fission chamber*

The factor f that converts the change in fission rate at the center to the whole reactor is verified. This is done by measuring the count rate at different positions of the fission chamber from the bottom reflector to the top reflector in a critical reactor (Figure 7). Because the reactor power cannot be kept perfectly steady the measured count rate is normalized with a monitor count rate determined with detector CFUM_667. This detector is located far from the experimental channel. which makes it unaffected by the movement of detector CFUF_34. Next the count rate is normalized to the maximum measured count rate.

Figure 20 and Table 16 give the normalized count rate when the fission chamber CFUF_34 is positioned at different heights in the reactor core. As expected, the count rate is highest in the middle of the active fuel part at a position of 307 mm. When the detector is positioned between -200 mm and -72 mm it resides in the bottom lead reflector. Here. the neutron flux will decrease. The same applies when the detector is placed in the top reflector between 691 mm and higher. The first minimum is located around 0 mm which is when the fuel zone starts after the stainless-steel supporting grid. The second minimum is located at the upper boundary where the active fuel part passes into the stainless-steel top plate at 616 mm.

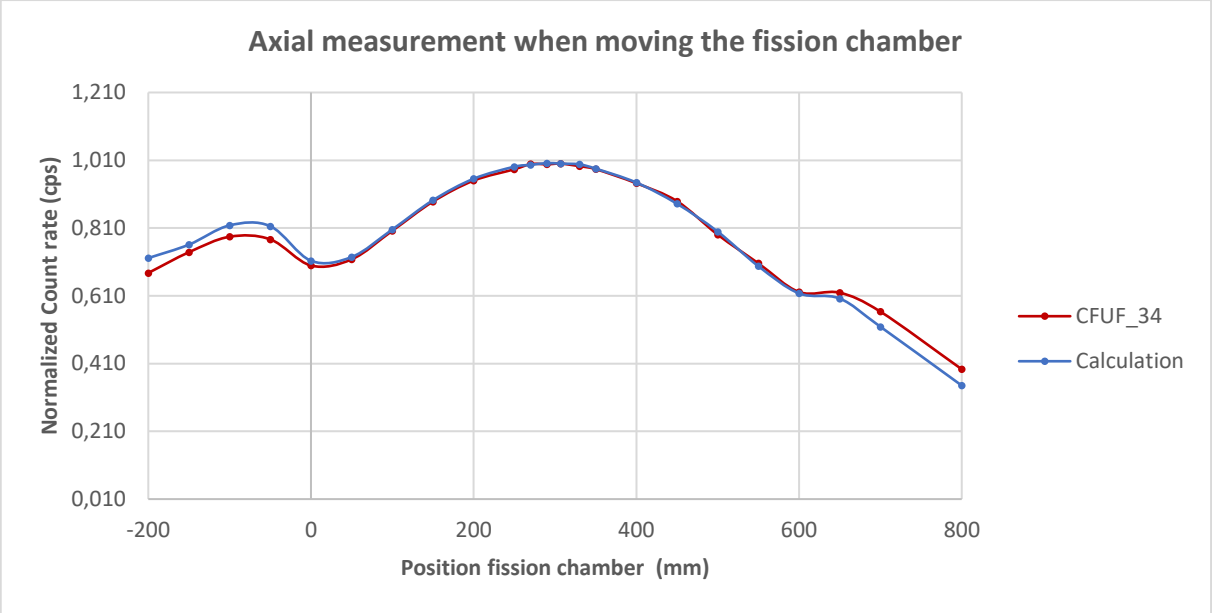

Figure 20: Count rate in function of the position of the fission chamber. normalized to the reactor power and to 1 in the core middle plane measured with a CFUF_34 fission chamber compared with calculation.

Table 16 also shows the results from the axial calculations and the relative difference between the normalized experimental results and calculations. As can be seen in Figure 20 the calculations are representative for the VENUS-F core with a relative difference from the experimental results below 1% for the positions of the detector between 50 mm and 450 mm. Under the position -50 mm and above 650 mm the relative difference between the calculations and the experiments rises above 5%. Thus, when the detector is no longer placed in the active fuel part there will be a higher relative difference between the calculations and the experimental results.

The calculations of the factor *f* are performed in the three subcritical cores with the Cf source present. The calculated values are shown in Table 10.

7.1.5 Calculation of the effective neutron fraction

Table 10 gives the parameters which are measured or calculated to determine the delayed neutron fraction for a fast critical reactor core. The final values of β_{eff} measured in the three subcritical cores agree with each other within the uncertainties. The average value is 706 pcm. The uncertainties are presented in Table 11. They consist of the uncertainty of the calibrated Cf source intensity, the statistical uncertainties of the measurements, the uncertainties of the evaluated nuclear data libraries, uncertainties of the fitting procedures and uncertainties of Monte Carlo calculations. All the uncertainties are combined together in quadrature and lead to the total uncertainty of about 5%.

Table 10: Determined parameters of the californium source method corresponding to their respective subcriticality level to calculate the delayed neutron fraction.

ρ (cents)	-13.71	-19.03	-23.96
S_{Cf}	375000	375000	375000
Q_f	1793.48	1298.29	1039.41
$\overline{\nu}$	2.51169	2.51169	2.51169
f	1.01E+05	1.00E+05	1.02E+05
$F^+_{\chi.\ Cf}(0)/\overline{F^+_\chi}$	1.183	1.183	1.183
β_{eff}	710	713	695

Table 11: Determined uncertainty on the parameters of the californium source method corresponding to their respective subcriticality level.

ρ (cents)	-13.71	-19.03	-23.96
Rel. Uncert ρ (%)	2.65	2.65	2.65
Rel. Uncert. S_{Cf} (%)	1.5	1.5	1.5
Rel. Uncert. Q_f (%)	1.56	1.75	1.82
Rel. Uncert. $\overline{\nu}$ (%)	0.00016	0.00016	0.00016
Rel. Uncert. F (%)	2.0	2.0	2.0
Rel. Uncert. $F^+_{\chi.\ Cf}(0)/\overline{F^+_\chi}$ (%)	2.0	2.0	2.0
Rel. Uncert. β_{eff} (%)	4.4	4.5	4.5
Abs. Uncert. β_{eff} (pcm)	32	32	32

7.2 DETERMINATION OF THE MEAN NEUTRON GENERATION TIME

Figure 47 to Figure 53 give the data and the fitted curves of the Rossi-α experiments. The measurements were executed on two days with 3 different detectors (RS_72, RS_79 and CFUL_600). The data can be fitted with an exponential that provides the prompt neutron decay constant α. The signals received by the PHSPA are processed in such a way that the neutrons measured in a certain time are stored in the corresponding bin. Each bin has a width of 10 μs so that the correlations between the neutrons are clearly displayed without being subjected to too many fluctuations. However, because of the dead time, the first bins do not give a true picture. In Table 12 the calculated α's are displayed if the first three, four and five bins are omitted. The results lie closest when the first five bins are left out. The uncertainties of the exponential fit with MATLAB is around 3%. All five values agree within this uncertainty.

Table 12: Determined alpha (prompt neutron decay constant) when the first three to five bins are excluded. The measurement took place in criticality.

Critical	Detector	α_3 (1/s)	α_4 (1/s)	α_5 (1/s)
DAY1	RS_79	2771	2605	2583
DAY1	CFUL_600	2594	2485	2438
DAY1	RS_72	2962	2655	2559
DAY2	RS_72	3742	2792	2491
DAY2	RS_79	2997	2737	2595

Table 13 shows the calculated prompt neutron decay constant for the measurements with two subcriticality levels when CR1 is positioned at 250 mm and 200 mm. For these measurements. detector RS_79 is used. Because of the subcriticality the decay constant needs to be normalized to a critical reactor core. When the first five bins are left out this results in an α of respectively 2374 s^{-1} and 2732 s^{-1} for the positions at 250 mm and 200 mm. These values differ by about 2 s of the uncertainty from the average of the values measured in the critical core. However, each of them differs in an opposite direction and the average value of the seven measurements equals 2539 s^{-1}.

Table 13: Determined alpha (prompt neutron decay constant) when the first three to five bins are excluded. The measurement took place in two subcriticality levels and alpha was normalized to criticality.

Subcrit	α_3 (1/s)	Norm. α_3 (1/s)	α_4 (1/s)	Norm. α_4 (1/s)	α_5 (1/s)	Norm. α_5 (1/s)
ρ_250	2823	2372	2809	2360	2826	2374
ρ_200	3259	2629	3316	2675	3387	2732

The average values of β_{eff} and α can be used in equation (18) to determine Λ. The final result equals to 2781 ns with an uncertainty of about 5%.

8 DISCUSSION

The effective delayed neutron fraction β_{eff} is determined using various parameters, some of them experimental and some of them calculated. In this chapter, the discrepancies between the calculations and experiments are discussed as well as the uncertainties and the possibilities for their reduction. First, the strength of the Cf-source is known from the certificate and its uncertainty has a value of 1.5% typical for such type of neutron source. It can be found in the literature that Cf neutron sources may be calibrated to an uncertainty of 1.1%.

The reactivity in dollar was measured for three subcriticality levels. The total uncertainty on the reactivity is mainly determined by the uncertainty of the nuclear data libraries. The uncertainties associated with the calculation of the abundance of precursor groups by Serpent2, statistical uncertainties of the measured count rates and the uncertainties of the least squares fits are relatively low.

The change in fission rate Q_f in the centre of the core is measured. After normalisation of the measured count rate, it is observed that for the three subcriticality levels the data are in a good agreement. The sources of uncertainties are the effective mass of the calibrated fission chamber, statistical uncertainties on the number of detected counts during the measurement with the source and during the background measurement. The standard deviation of the count rate determined for different discrimination levels is also taken into account. Due to a low count rate, each measurement took about one hour. This type of a measurement is rather sensitive to perturbations, for example electronic noise, which can seriously impact the measured spectra (see an example in Figure 43). Therefore, it would be beneficial if the measurement conditions are such that a single measurement takes shorter time. For example, using a stronger Cf-source or a fission chamber with a heavier deposit or calibrating the measurement with a monitor detector having a bigger count rate would enable to shorten the measurement time and to increase the counting statistics.

The average number of neutrons emitted per fission $\bar{\nu}$ was calculated with Serpent2. As this value is averaged over the entire reactor, its uncertainty is very small.

The axial calculations in which the fission chamber is moved give results that coincide very well with the experimental results. The deviation from the experimental results is only significant when the detector is placed in the bottom and top lead reflectors. The calculation of the fission rate in the entire core has a very small uncertainty. However, the calculation of the fission rate in a small volume of the fission chamber deposit has dominant statistical uncertainty. Moreover, the source driven calculations in subcritical states that are very close to criticality are extremely time consuming because the fission chains are long.

Concerning the axial calculations in which the Cf source is moved through the reactor core, it can be concluded that the general trend set by the experimental results is followed. The calculations suffer from big statistical uncertainties because of the proximity to the critical state as explained in the previous paragraph. Additionally, simulating detectors located in the outer reflector where the neutron flux is low brings additional statistical uncertainty.

Overall, the β_{eff} uncertainty of about 5% is comparable with the values found in literature, which are usually between 3% and 4%. Considering the above mentioned suggestions and their application in next measurements could decrease the uncertainty of the final value. The experimental β_{eff} value determined with the Cf source method is 6% smaller than the value calculated using Serpent2, which means agreement within 2σ.

Using this β_{eff} value and additional Rossi-alpha measurement for the prompt neutron decay constant α enables to determine the neutron generation time Λ. The experimental value is about 30% bigger than the calculation, which represent about 6σ. It will be necessary to dedicate further investigation to this part of the experiment.

9 CONCLUSION

In this work, a measurement system for determination of the effective delayed neutron fraction β_{eff} using the ^{252}Cf-source method was developed and tested at the zero-power VENUS-F reactor. Additional experiments were made using the Rossi-α neutron noise method for measurement of the prompt neutron decay constant α. These two approaches together enable determination of the mean neutron generation time Λ. Monte Carlo simulations with the Serpent2 code were performed to calculate correction factors and the kinetic parameters for comparison with the experiments. A complex assessment of sources of uncertainties was also made.

The measurement system consists of the californium source, a remotely controlled moving mechanism (which enables moving the source axially through the fuel zone and top reflector), a miniature fission chamber with calibrated effective mass (~ 3 mg ^{235}U), neuron flux monitors (placed in the reflector) and data acquisition system. The latter comprises the GENIE-2000 software for recording spectrum of fission fragments and a LabVIEW-based software for recording count rates of multiple detectors.

A geometry model of the investigated reactor configuration was created in the Serpent2 code. It was used for criticality calculations to determine k_{eff}, delayed neutron parameters, average number of neutrons emitted per fission $\bar{\nu}$ as well as for source driven calculations with the ^{252}Cf source to determine changes in fission rates in the reactor core depending on the ^{252}Cf source position and core reactivity.

Measurements with the ^{252}Cf-source method were performed at three subcriticality levels -0.137 $, -0.190 $ and -0.240 $. The product of the reactivity and the central fission rate measured with the calibrated fission chamber at the three subcriticality levels agree within the statistical uncertainties. After application of the calculated parameters, the final value of β_{eff} was determined to be (706 ± 32) pcm. Serpent2 gives a value that is about 6% bigger, which agrees with the experiment within 2σ.

The mean neutron generation time was determined based on the β_{eff} value from the Cf-source method and the α value from the Rossi-α method measured in a critical and two subcritical states. The final value of Λ is (2781 ± 150) ns. Serpent2 gives a value that is 29% smaller, which represents more than 5σ. That indicates either a problem in the simulation or in the application of the Rossi-α method, which requires further investigation.

REFERENCES

[1] SCK CEN. 'Exploring a better tomorrow | SCK CEN'. https://www.sckcen.be/nl (accessed Mar. 29. 2021).

[2] Nuclear Power Web. 'Nuclear Power for Everybody - What is Nuclear Power'. https://www.nuclear-power.net/ (accessed Mar. 25. 2021).

[3] M. Serge. *The physics of nuclear reactors*. Cham: Springer International Publishing. 2017.

[4] G. E. Mckenzie IV. 'Modern Rossi Alpha Measurements'. Univerity of Illinois. 2014.

[5] OECD / NEA Data Bank. 'JANIS'. https://www.oecd-nea.org/janisweb/tree (accessed Nov. 25. 2020).

[6] M. Akbari. S. Rezaei. and F. Khoshahval. 'Kinetic Parameters Calculation During First Cycle of the Wwer-1000 Reactor Core'. *CNL Nucl. Rev.*. vol. 8. no. 1. pp. 63–70. 2019. doi: 10.12943/cnr.2017.00017.

[7] IAEA: education and training. 'PHYSICS AND KINETICS OF TRIGA REACTORS'. 2004. https://ansn.iaea.org/Common/documents/Training/TRIGA Reactors (Safety and Technology)/chapter2/physics214.htm (accessed Jan. 08. 2021).

[8] A. Kochetkov. G. Vittiglio. J. Wagemans. W. Uyttenhove. A. Krása. and J. Hernandez. 'The Lead-Based VENUS-F Facility: Status of the FREYA Project'. in *EPJ Web of Conferences*. Feb. 2016. vol. 106. doi: 10.1051/epjconf/201610606004.

[9] J. Wagemans. L. Borms. A. Kochetkov. A. Krása. C. Van Grieken. and G. Vittiglio. 'Nuclear instrumentation in VENUS-F'. in *EPJ Web of Conferences*. Jan. 2018. vol. 170. doi: 10.1051/epjconf/201817004027.

[10] J. E. Martin. *Physics for Radiation Protection*. Thirth Edi. Weinheim: Wiley-VCH. 2016.

[11] R. C. Martin. J. B. Knauer. and P. A. Balo. 'Production. distribution and applications of californium-252 neutron sources'. *Appl. Radiat. Isot.*. vol. 53. no. 4–5. pp. 785–792. 2000. doi: 10.1016/S0969-8043(00)00214-1.

[12] J. Coburn. S. M. Luker. E. J. Parma. and K. R. DePriest. 'Modeling. Calibration. and Verification of a Fission Chamber for ACRR Experimenters'. *EPJ Web Conf.*. vol. 106. 2016. doi: 10.1051/epjconf/201610605001.

[13] G. de Izarra. 'COSICAF. a fission chamber simulation tool for academic purposes'. *EPJ Nucl. Sci. Technol.*. vol. 6. p. 49. 2020. doi: 10.1051/epjn/2020011.

[14] S. Ahmed. 'Gas-filled detectors'. in *Physics and Engineering of Radiation Detection*. 2de editio.. Amsterdam: Elsevier Ltd. 2015. pp. 157–231.

[15] V. Lamirand *et al.*. 'Intercomparison of neutron noise measurement systems in the CROCUS reactor'. *Proc. PHYSOR 2018*. no. April. p. 11. 2018.

[16] V. A. Doulin. G. M. Mikhailov. A. L. Kotchetkov. I. P. Matveenko. and S. P. Belov. 'THE βeff MEASUREMENT RESULTS ON FCA-XIX CORES'. 1999. [Online]. Available: www.elsevier.com/locate/pnucene.

[17] S. G. Carpenter. J. M. Gasidlo. and J. M. Stevenson. 'Measurements of the Effective Delayed-Neutron Fraction in Two Fast Critical Experiments'. *Nucl. Sci. Eng.*. vol. 49. no. 2. pp. 236–239. 1972. doi: 10.13182/nse72-2.

[18] E. A. Fischer. 'Integral measurements of the effective delayed neutron fractions in the fast critical assembly SNEAK'. *Nucl. Sci. Eng.*. vol. 62. pp. 105–116. 1977.

[19] T. Sakurai. S. Okajima. H. Song. and Y.-I. Kim. 'Measurement of Effective Delayed Neutron Fraction βeff by 252Cf Source Method for Benchmark Experiments of βeff at FCA'. 1999. [Online]. Available: www.elsevier.com/locate/pnucene.

[20] J. Leppänen. 'Development of a new Monte Carlo reactor physics code'. 2007.

[21] J. Leppänen. M. Pusa. T. Viitanen. V. Valtavirta. and T. Kaltiaisenaho. 'The Serpent Monte Carlo code: Status. development and applications in 2013'. *Ann. Nucl. Energy*. vol. 82. pp. 142–150. 2015. doi: 10.1016/j.anucene.2014.08.024.

[22] Y. Nauchi and T. Kameyama. 'Development of calculation technique for iterated fission probability and reactor kinetic parameters using continuous-energy monte carlo method'. *J. Nucl. Sci. Technol.*. vol. 47. no. 11. pp. 977–990. 2010. doi: 10.1080/18811248.2010.9711662.

[23] J. Leppänen. M. Aufiero. E. Fridman. R. Rachamin. and S. Van Der Marck. 'Calculation of

effective point kinetics parameters in the Serpent 2 Monte Carlo code'. *Ann. Nucl. Energy*. vol. 65. pp. 272–279. 2014. doi: 10.1016/j.anucene.2013.10.032.
[24] Photonis;. 'Photonis'. 2021. https://www.photonis.com/ (accessed May 18. 2021).
[25] N. Blanc De Lanaute. 'Mode Operatoire (MO) Spectre'.
[26] FSUE State Scientific Centre of Russia. 'Certificate No. 8644 for radioactive source'. Dimitrovgrad. 2004.
[27] J. Magill. G. Pfenning. R. Dreher. and Z. Sóti. *Karlsruher nuklidkarte*. 9th Editio. Nucleonica. 2015.
[28] National Nuclear Data Center. 'Nudat 2'. https://www.nndc.bnl.gov/nudat2/reCenter.jsp?z=98&n= 154 (accessed Dec. 08. 2020).
[29] D. ; Rozon. 'Chapter 2 The Diffusion Equation and the Steady State'. in *Introduction to nuclear reactor kinetics*. Montreal: Polytechnic International Press. 1998. pp. 26–75.

ANNEX A:

A1 STRENGTH OF THE SOURCE

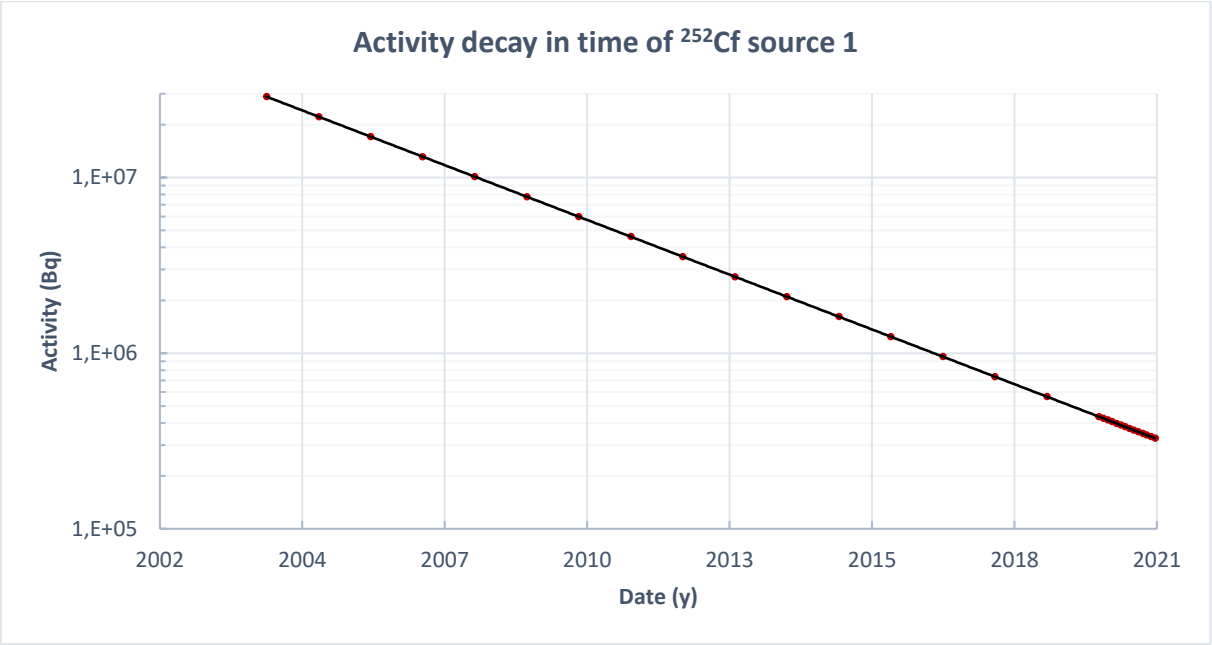

Figure 21: Exponential decrease of the activity of ^{252}Cf source 1 from its calibration day to the year of measurement.

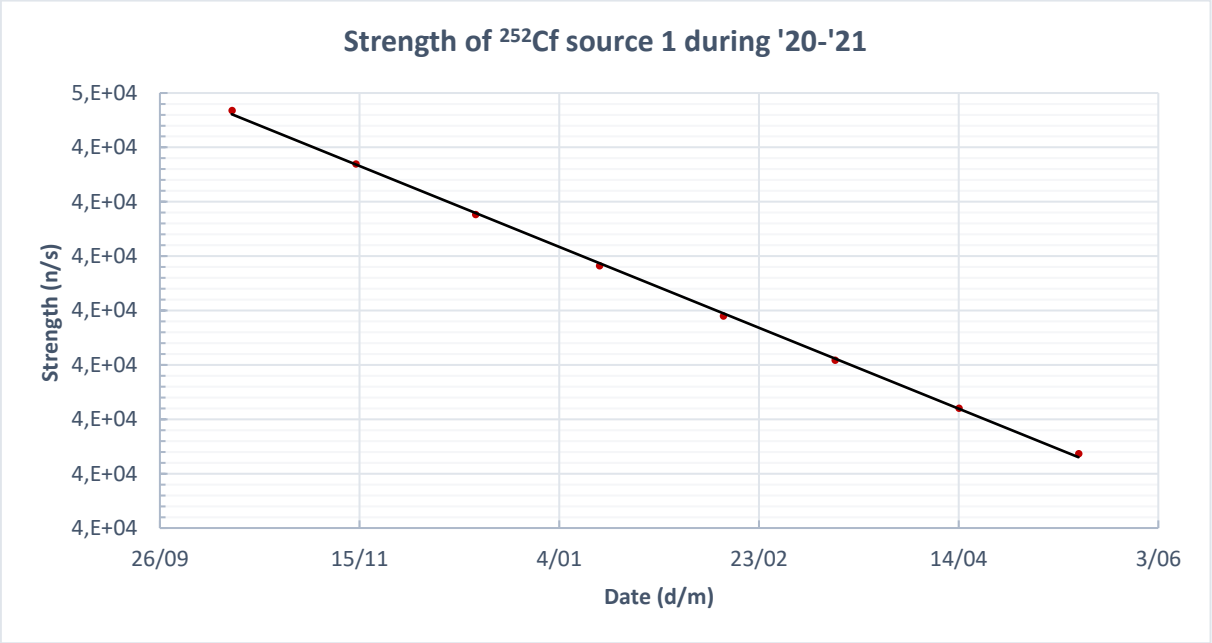

Figure 22: Detailed view of the decrease in strength of ^{252}Cf source 1 during the academic year of the measurements.

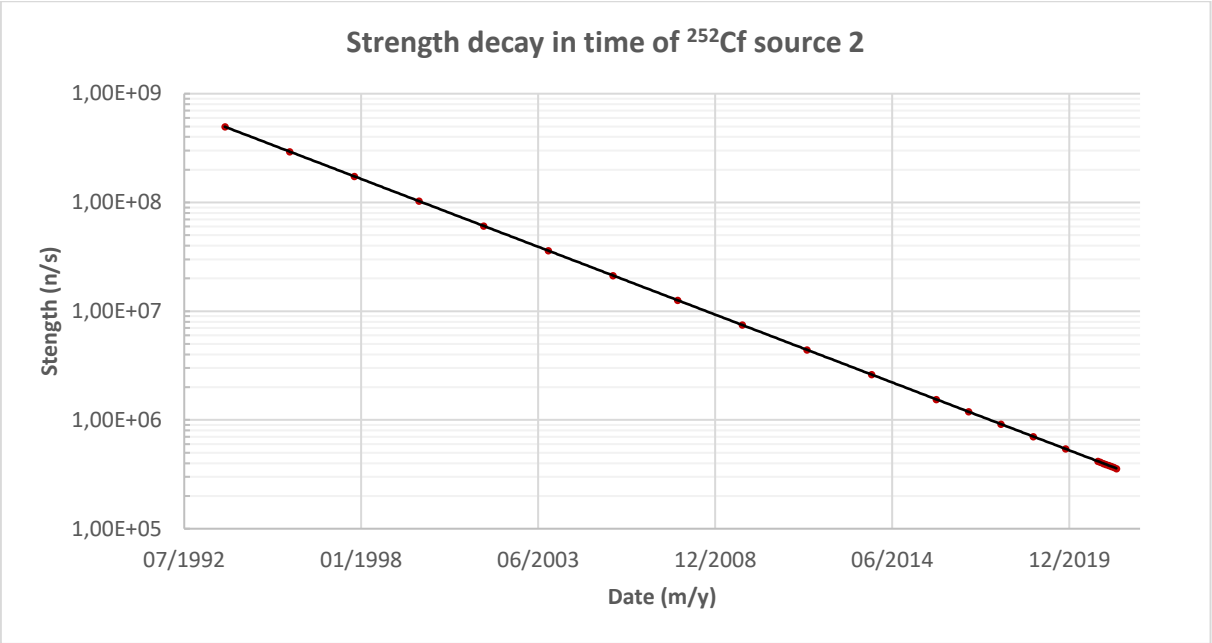

Figure 23: Exponential decrease of the strength of ^{252}Cf source 2 from its calibration day to the year of measurement.

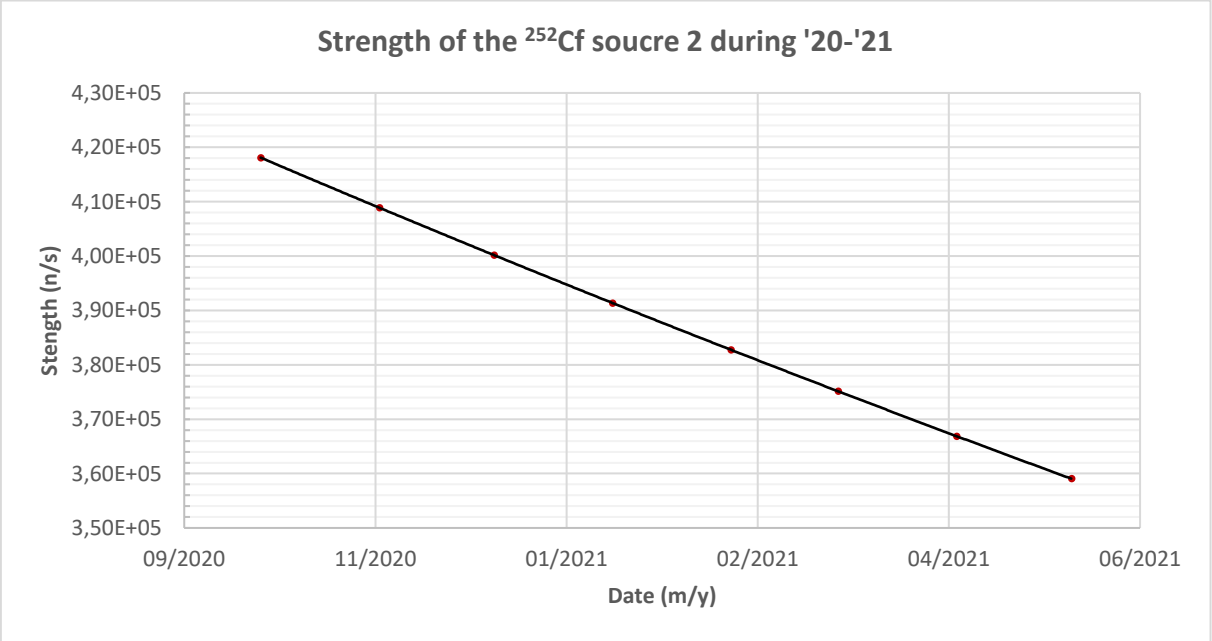

Figure 24: Detailed view of the decrease in strength of ^{252}Cf source 2 during the academic year of the measurements.

A2 CALIBRATION CONTROL RODS

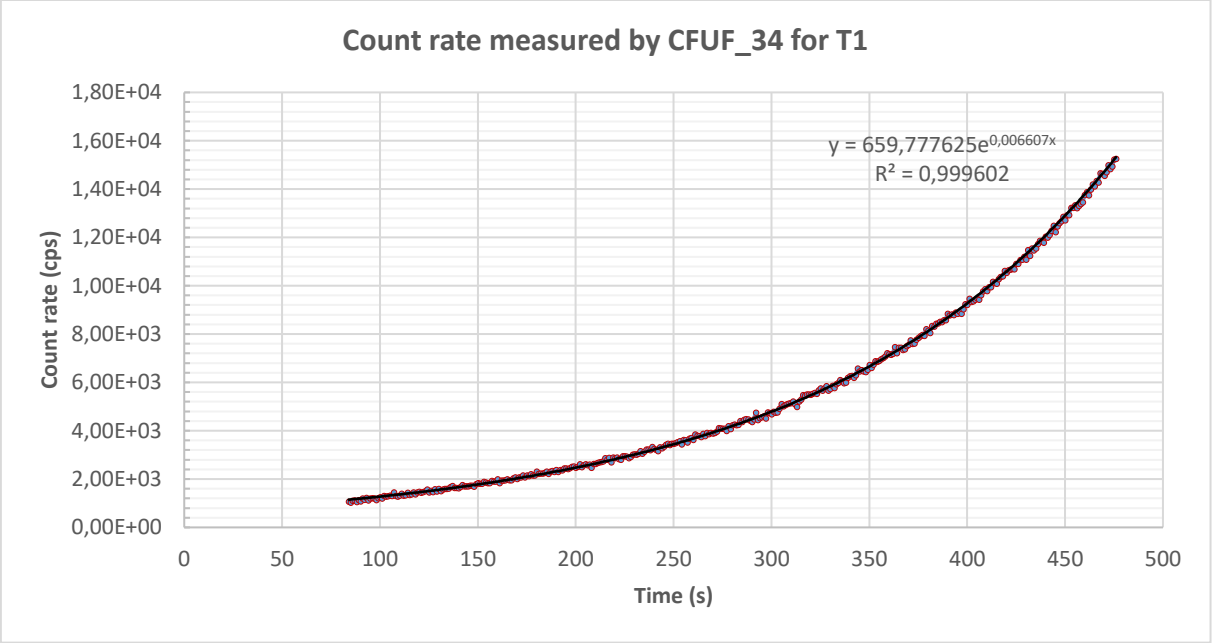

Figure 25: Count rate measured by CFUF_34 during exponential reactor period T1 with CR1@500mm and CR2@428mm.

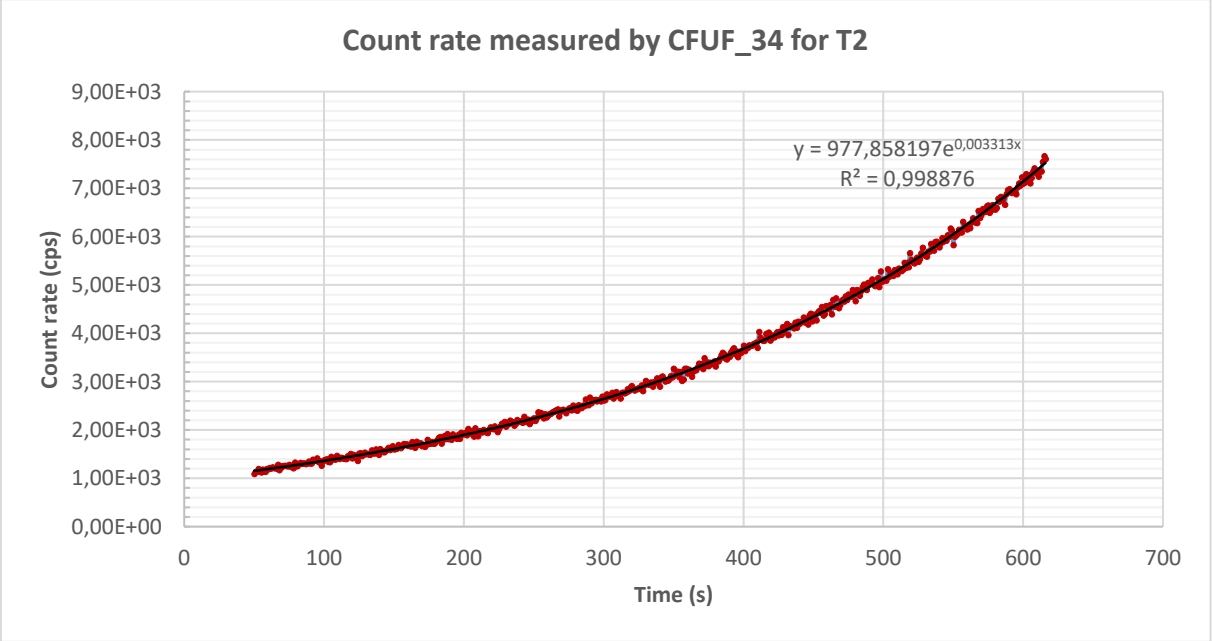

Figure 26: Count rate measured by CFUF_34 during exponential reactor period T2 with CR1@550mm and CR2@395mm.

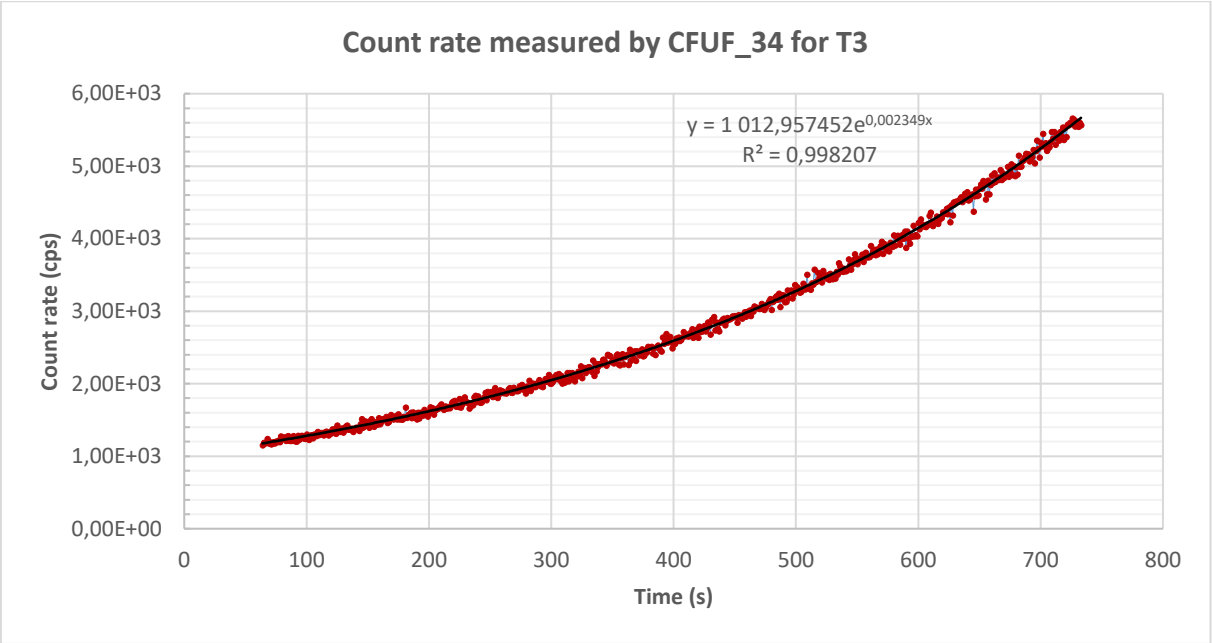

Figure 27: Count rate measured by CFUF_34 during exponential reactor period T3 with CR1@600mm and CR2@378mm.

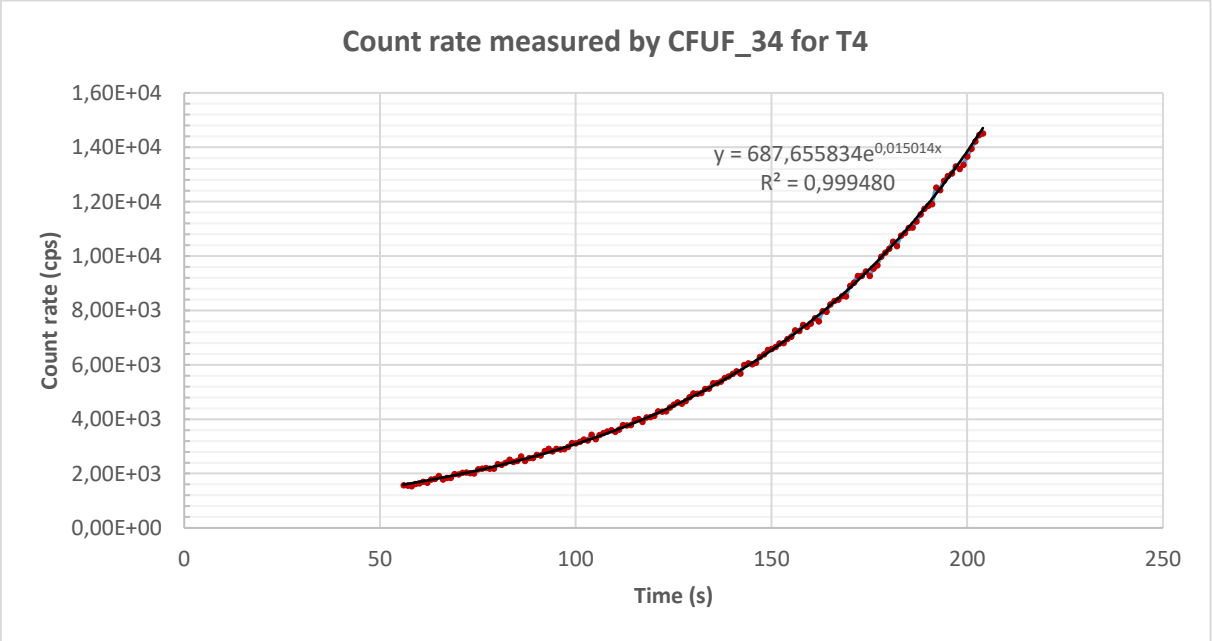

Figure 28: Count rate measured by CFUF_34 during exponential reactor period T4 with CR1@428mm and CR2@500mm.

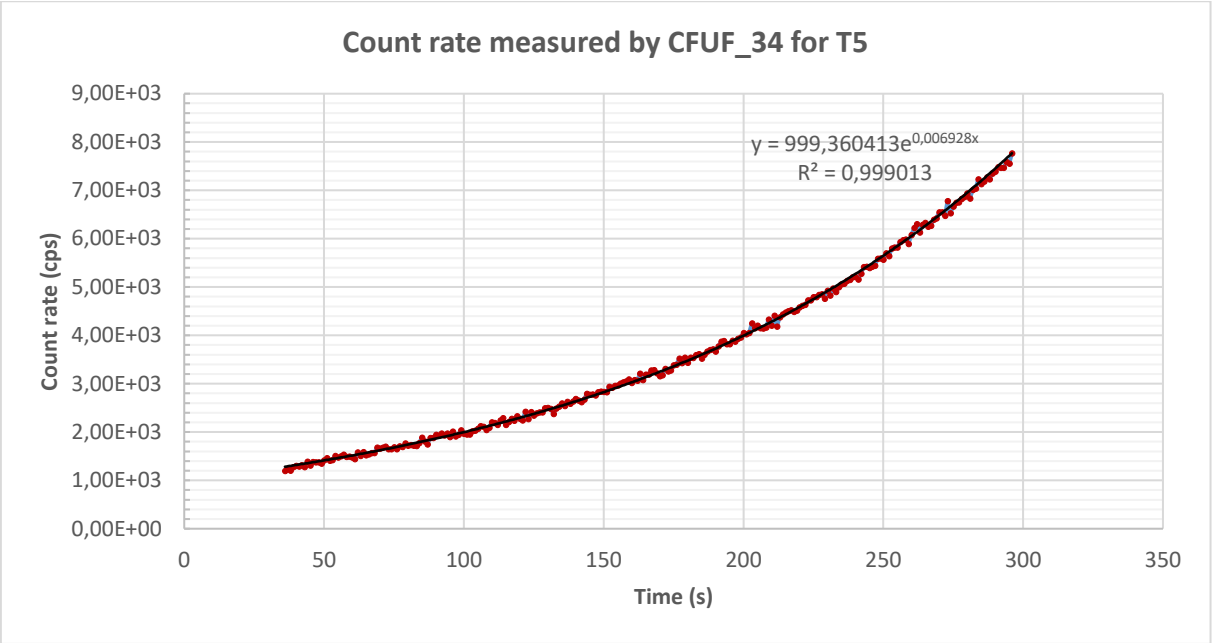

Figure 29: Count rate measured by CFUF_34 during exponential reactor period T5 with CR1@313mm and CR2@550mm.

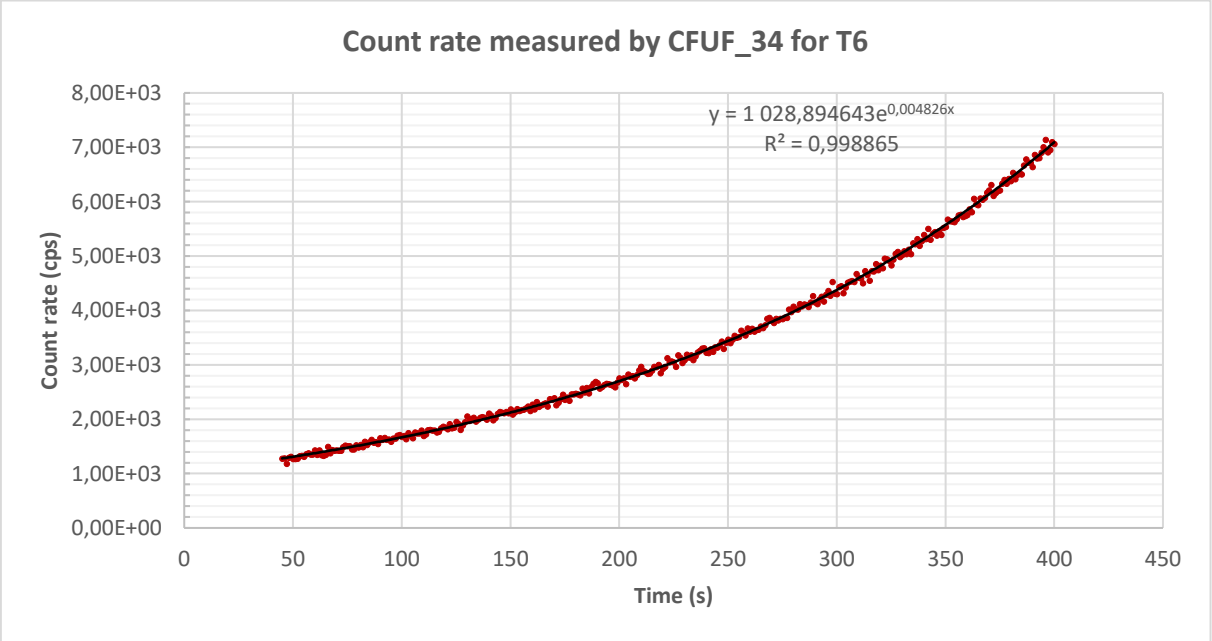

Figure 30: Count rate measured by CFUF_34 during exponential reactor period T6 with CR1@250mm and CR2@600mm.

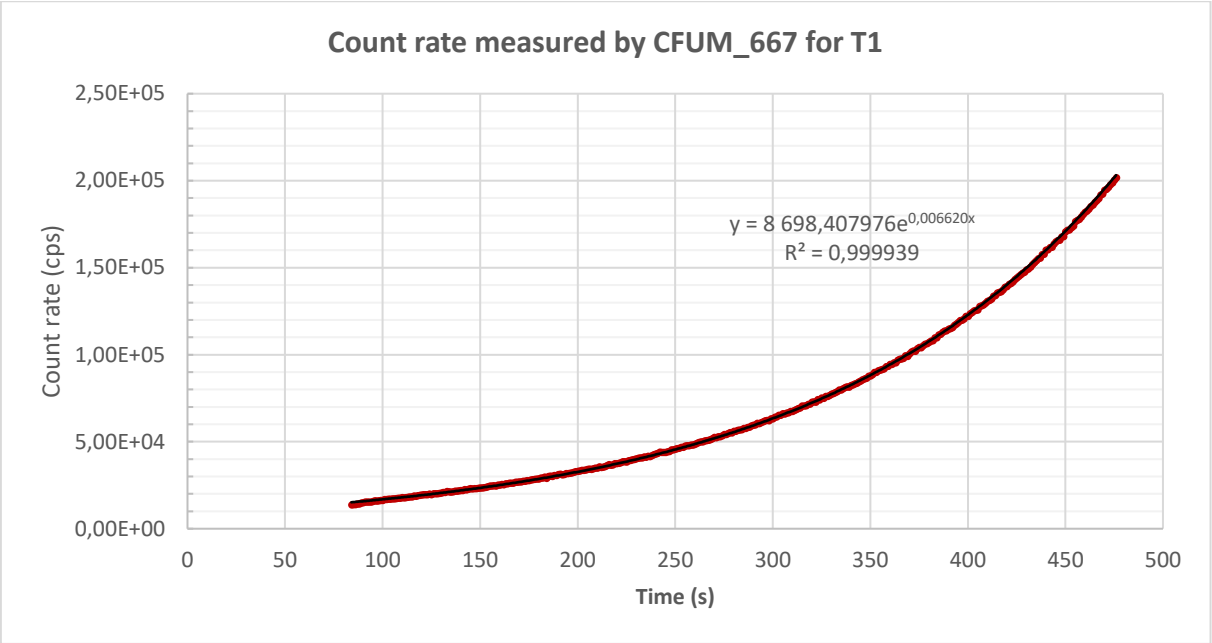

Figure 31: Count rate measured by CFUM_667 during exponential reactor period T1 with CR1@500mm and CR2@428mm.

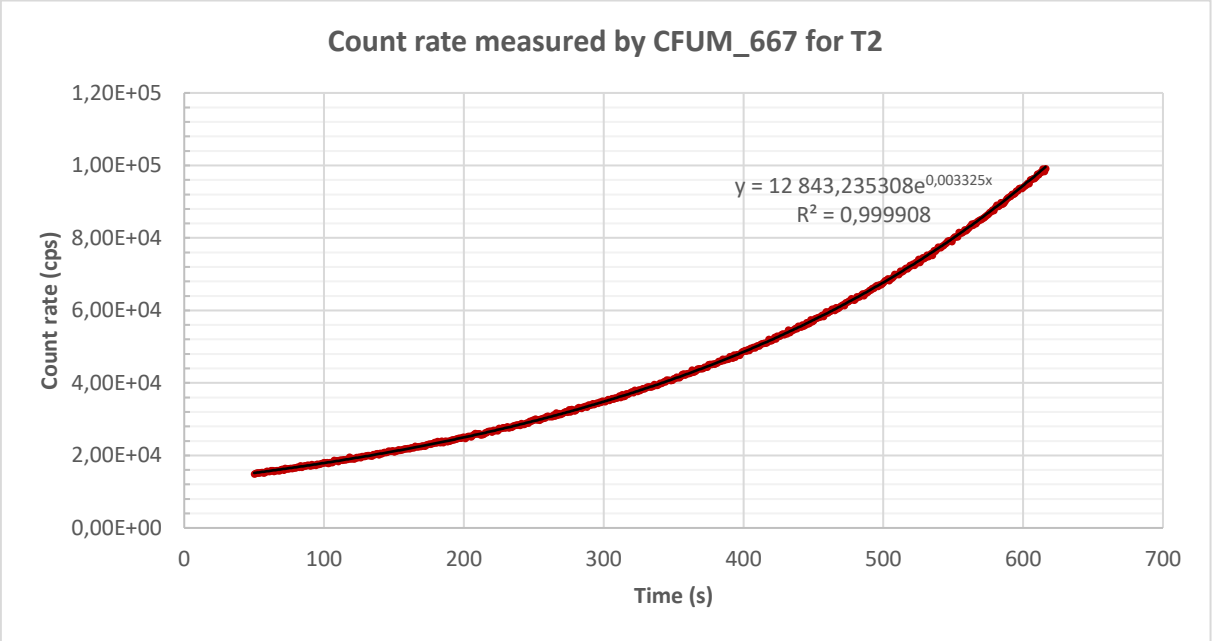

Figure 32: Count rate measured by CFUM_667 during exponential reactor period T2 with CR1@550mm and CR2@395mm.

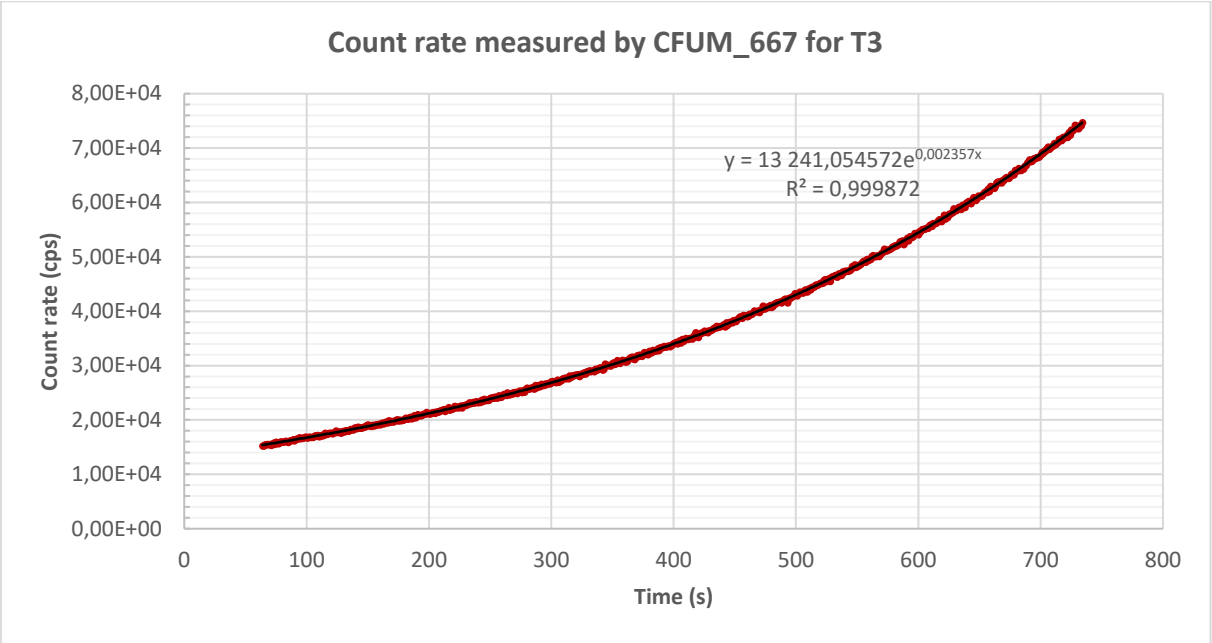

Figure 33: Count rate measured by CFUM_667 during exponential reactor period T3 with CR1@600mm and CR2@378mm.

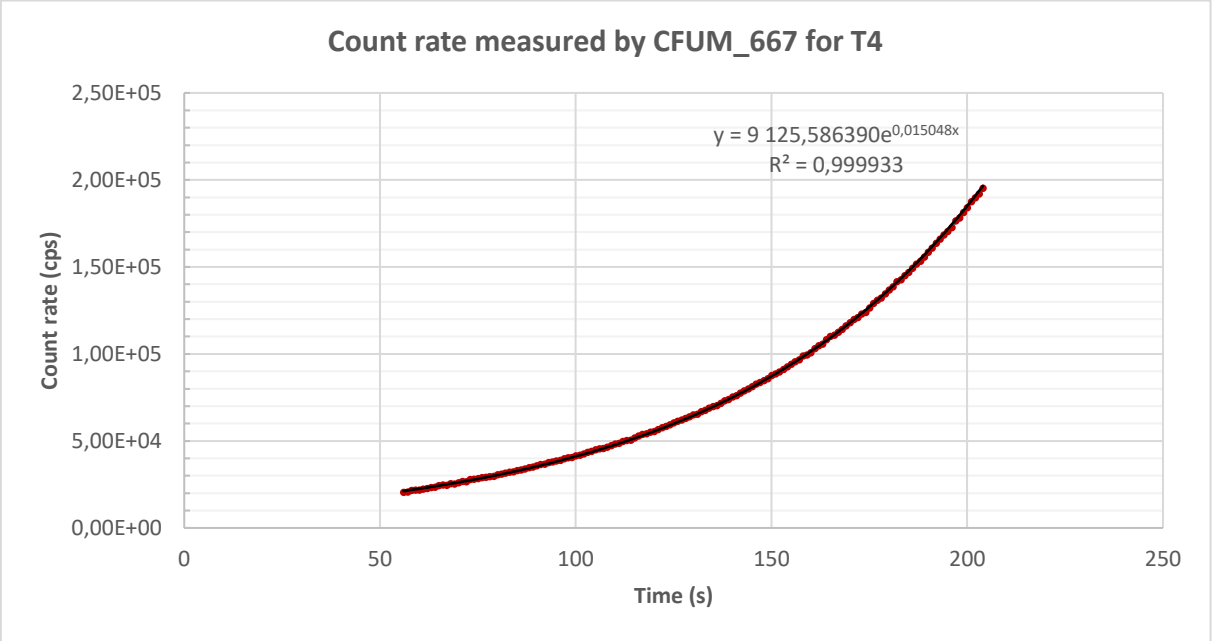

Figure 34: Count rate measured by CFUM_667 during exponential reactor period T4 with CR1@428mm and CR2@500mm.

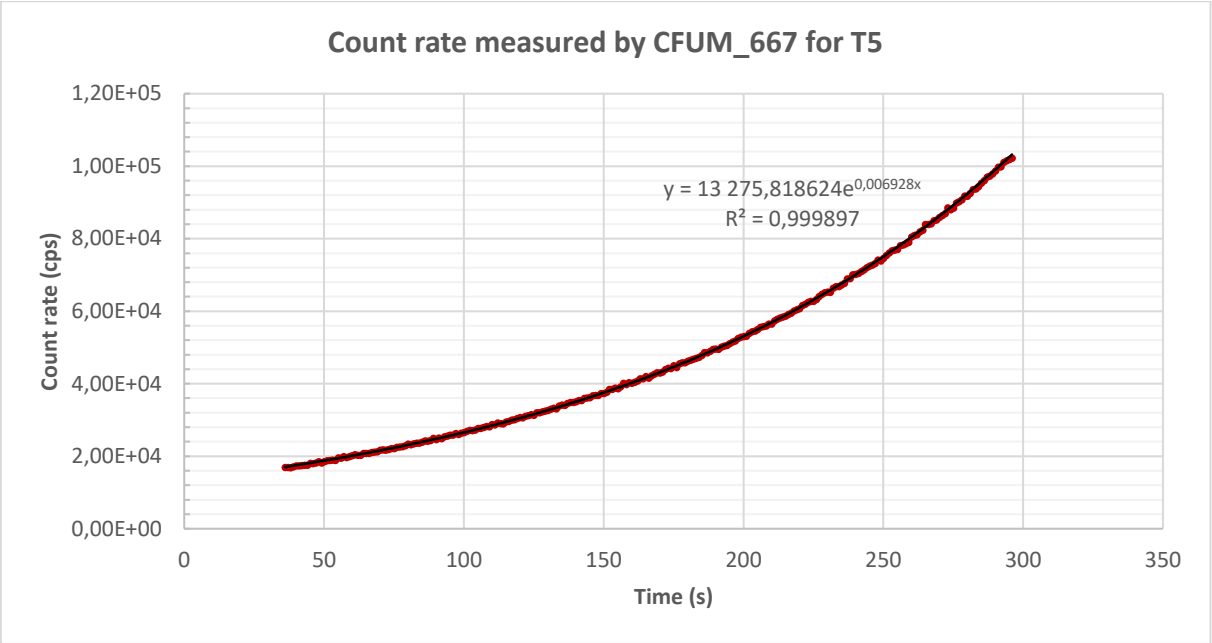

Figure 35: Count rate measured by CFUM_667 during exponential reactor period T5 with CR1@313mm and CR2@550mm.

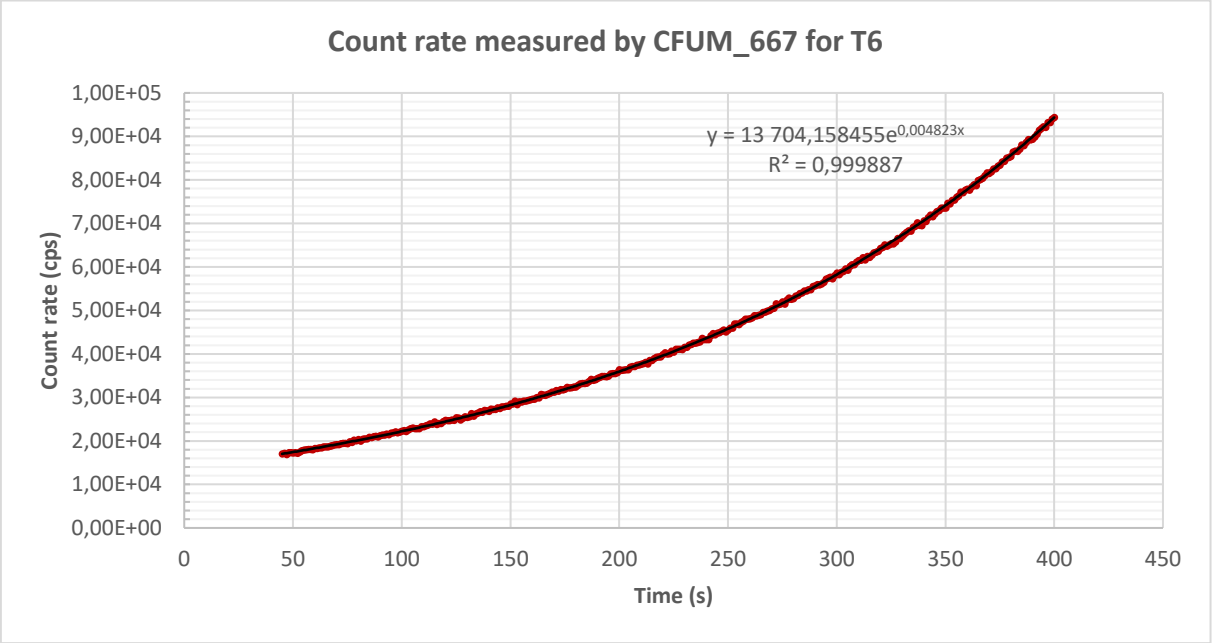

Figure 36: Count rate measured by CFUM_667 during exponential reactor period T6 with CR1@250mm and CR2@600mm.

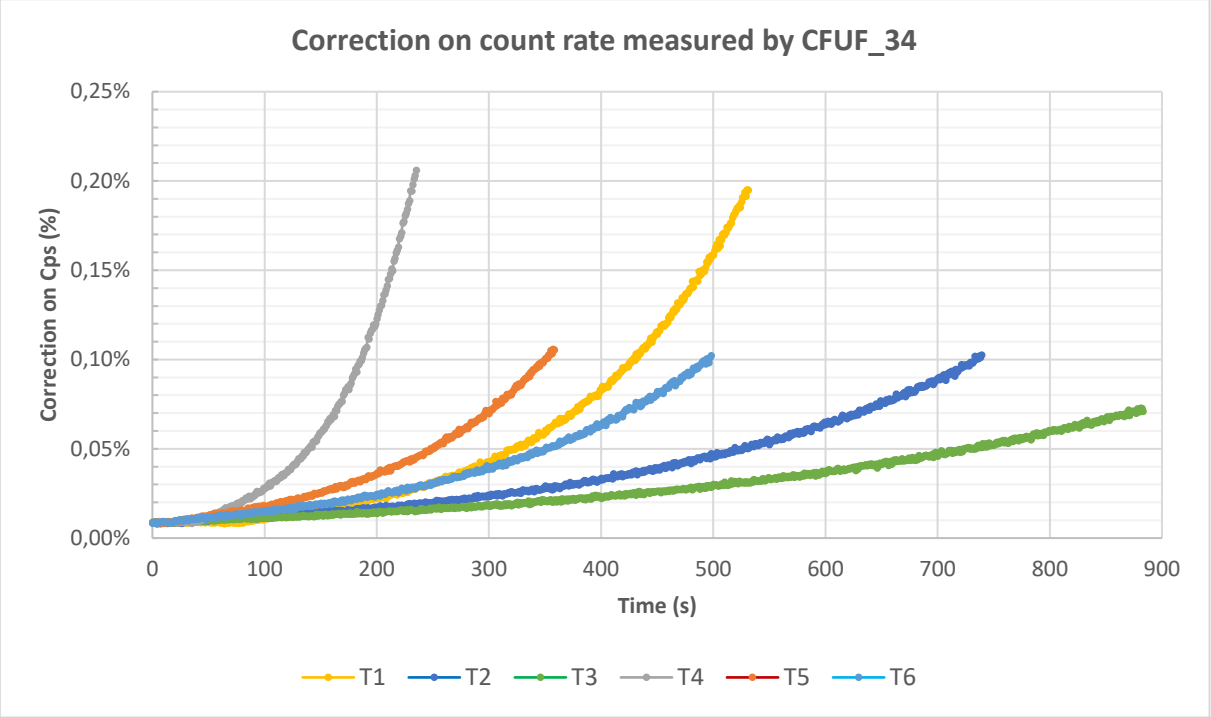

Figure 37: Correction due to dead time on count rate measured by CFUF_34 during exponential reactor periods T1 to T6.

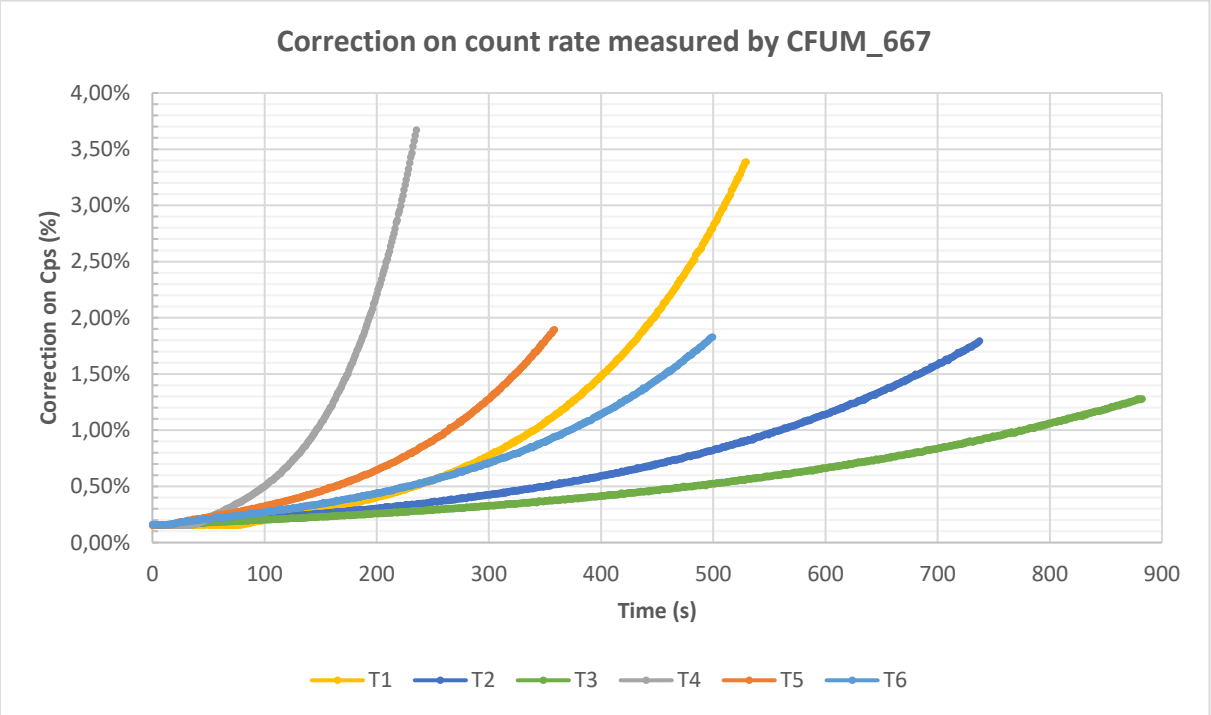

Figure 38: Correction due to dead time on count rate measured by CFUF_34 during exponential reactor periods T1 to T6.

A3 CHANGE IN FISSION RATE

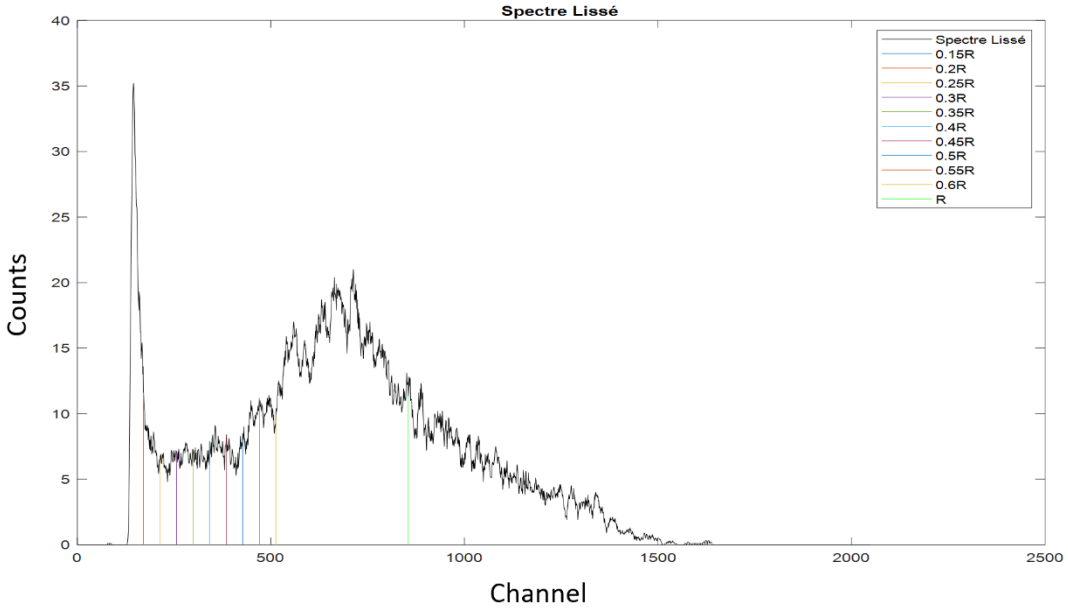

Figure 39: Smooth spectrum of fission fragments measured with FC_213 in subcriticality level 1 with GENIE-2000 located at SCK CEN. Different discrimination levels correspond with a calibrated effective mass of ^{235}U present in the detector. The counts per channel is plotted in function of the channel.

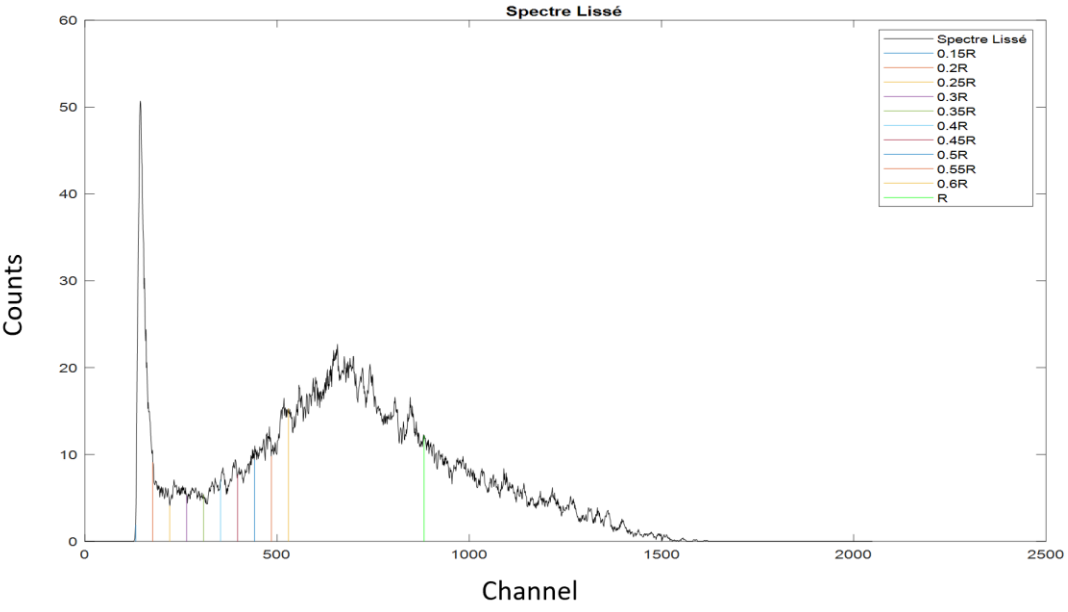

Figure 40: Smooth spectrum of fission fragments measured with FC_213 in subcriticality level 2 with GENIE-2000 located at SCK CEN. Different discrimination levels correspond with a calibrated effective mass of ^{235}U present in the detector. The counts per channel is plotted in function of the channel.

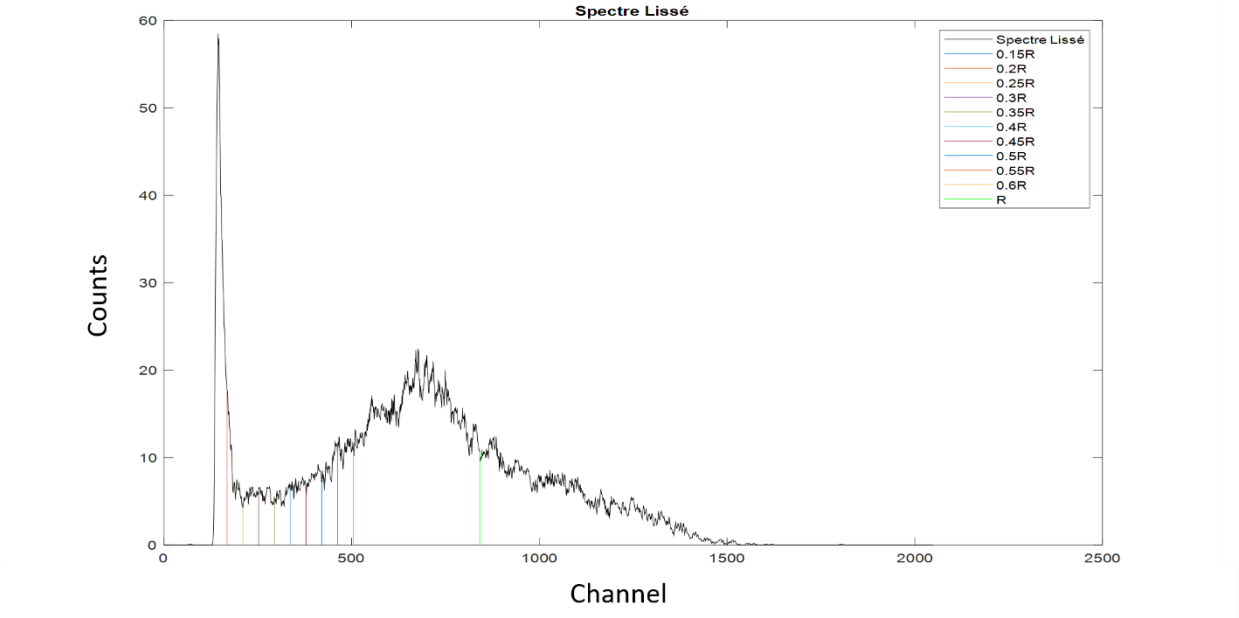

Figure 41: Smooth spectrum of fission fragments measured with FC_213 in subcriticality level 3 with GENIE-2000 located at SCK CEN. Different discrimination levels correspond with a calibrated effective mass of ^{235}U present in the detector. The counts per channel is plotted in function of the channel.

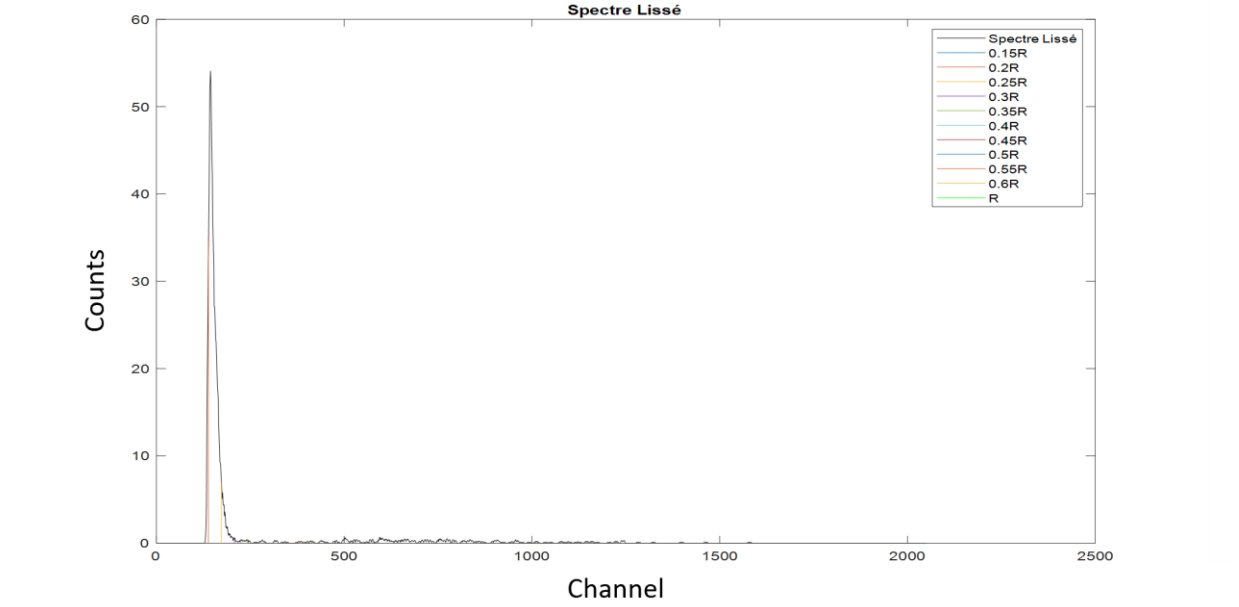

Figure 42: Smooth background spectrum of fission fragments measured with FC_213 in subcriticality level 1 with GENIE-2000 located at SCK CEN. Different discrimination levels correspond with a calibrated effective mass of ^{235}U present in the detector. The counts per channel is plotted in function of the channel.

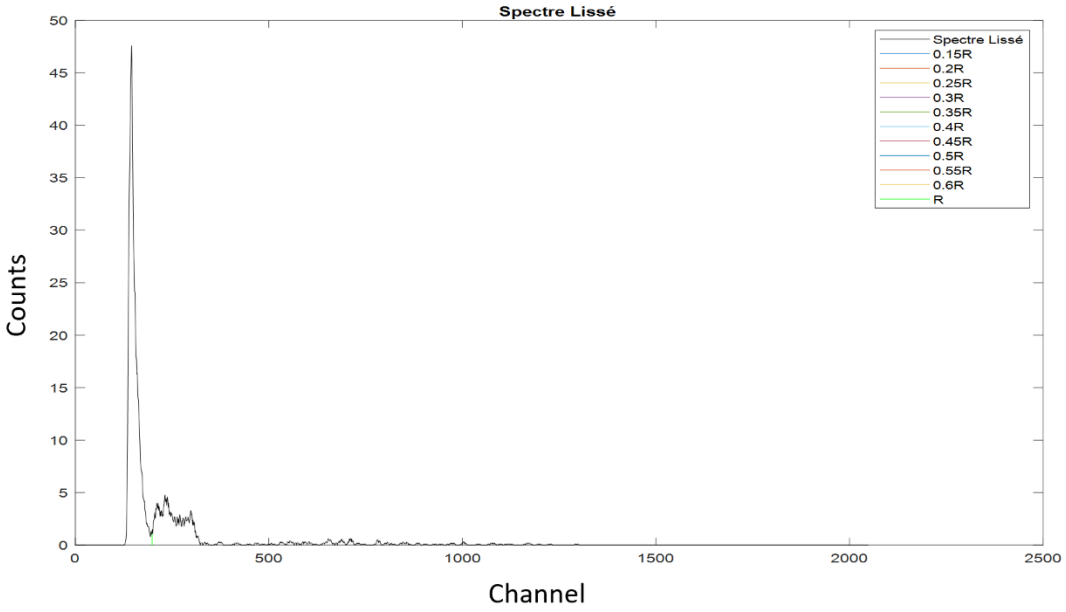

Figure 43: Smooth background spectrum of fission fragments measured with FC_213 in subcriticality level 2 with GENIE-2000 located at SCK CEN. Different discrimination levels correspond with a calibrated effective mass of ^{235}U present in the detector. The counts per channel is plotted in function of the channel.

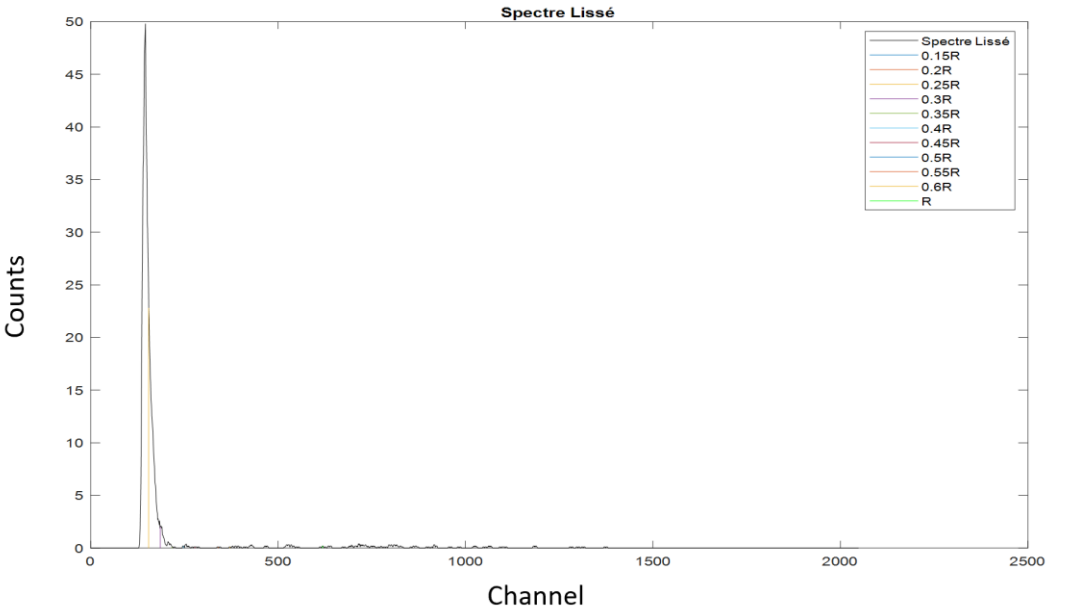

Figure 44: Smooth background spectrum of fission fragments measured with FC_213 in subcriticality level 3 with GENIE-2000 located at SCK CEN. Different discrimination levels correspond with a calibrated effective mass of ^{235}U present in the detector. The counts per channel is plotted in function of the channel.

A4 AXIAL MEASUREMENT WHEN MOVING THE CF SOURCE

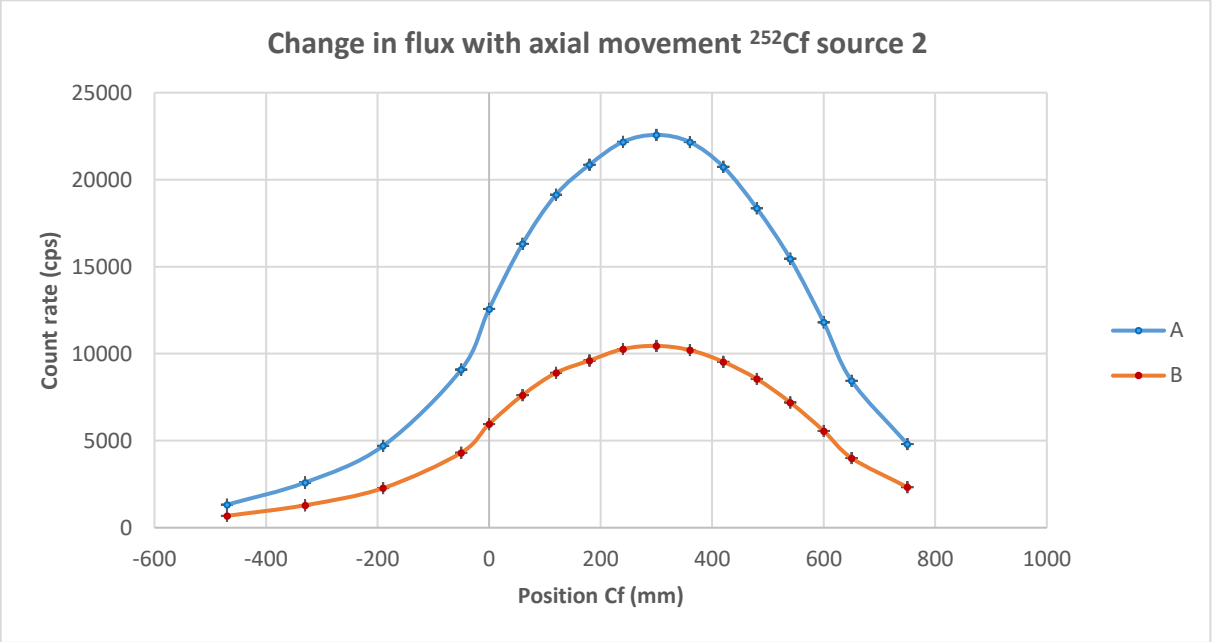

Figure 45: Count rate as a function of the position of ^{252}Cf source 2 when moving axially at reactivity of -13.71 cents.

Table 14: Measured count rate by detector A and B when moving the ^{252}Cf source 2 axially at reactivity of -13.71 cents. The count rate was averaged over five readings and normalized.

Position (mm)	A1	B1	A2	B2	A3	B3	A4	B4	A5	B5	Norm Av. A (cps)	Norm Av. B (cps)	Uncert A (%)	Uncert B (%)
-470	1344	691	1315	678	1315	679	1318	679	1316	670	0.06	0.07	2.75%	3.84%
-330	2584	1271	2586	1312	2567	1270	2655	1317	2587	1277	0.11	0.12	1.96%	2.79%
-190	4737	2285	4730	2283	4732	2276	4629	2295	4683	2236	0.21	0.22	1.46%	2.10%
-50	8977	4268	8972	4317	9146	4348	9169	4277	9168	4331	0.40	0.41	1.05%	1.52%
0	12507	5930	12574	5963	12646	5939	12543	5940	12597	5992	0.56	0.57	0.89%	1.30%
60	16251	7597	16380	7625	16338	7613	16290	7548	16310	7704	0.72	0.73	0.78%	1.15%
120	19263	8947	19130	8895	19014	8885	19095	8869	19169	8899	0.85	0.85	0.72%	1.06%
180	20666	9669	20871	9603	20784	9558	20976	9552	20996	9650	0.92	0.92	0.69%	1.02%
240	22023	10186	22314	10347	22250	10394	21784	10081	22499	10326	0.98	0.98	0.67%	0.99%
300	22508	10489	22776	10422	22492	10485	22547	10482	22542	10358	1.00	1.00	0.67%	0.98%
360	22110	10244	22370	10226	22148	10241	22051	10099	22128	10228	0.98	0.98	0.67%	0.99%
420	20829	9484	20795	9506	20635	9391	20616	9656	20826	9617	0.92	0.91	0.69%	1.02%
480	18280	8449	18386	8620	18526	8544	18286	8510	18313	8627	0.81	0.82	0.74%	1.08%
540	15513	7289	15433	7135	15414	7199	15424	7163	15514	7205	0.68	0.69	0.80%	1.18%
600	11919	5607	11932	5623	11787	5599	11764	5509	11611	5468	0.52	0.53	0.92%	1.34%
650	8543	4019	8369	3962	8319	3970	8516	4002	8463	4050	0.37	0.38	1.09%	1.58%
750	4788	2336	4793	2321	4768	2334	4799	2332	4885	2321	0.21	0.22	1.44%	2.07%

Table 15: Normalized calculated count rate with its absolute uncertainty and the relative error with the measured count rate at position B at reactivity of -13.71 cents.

Position (mm)	Norm Av. B (cps)	Norm calculation (cps)	Abs. Uncert (cps)	Rel. Error (%)
-470	0.07	0.04	0.01	-31%
-330	0.12	0.10	0.01	-17%
-190	0.22	0.21	0.02	-2%
-50	0.41	0.36	0.04	-14%
0	0.57	0.57	0.06	-1%
60	0.73	0.65	0.07	-12%
120	0.85	0.86	0.09	1%
180	0.92	1.01	0.11	10%
240	0.98	0.94	0.10	-4%
300	1.00	1.00	0.11	0%
360	0.98	1.01	0.11	4%
420	0.91	0.96	0.11	5%
480	0.82	0.74	0.08	-10%
540	0.69	0.81	0.09	17%
600	0.53	0.45	0.05	-15%
650	0.38	0.32	0.04	-17%
750	0.22	0.24	0.03	6%

A5 AXIAL MEASUREMENT WHEN MOVING THE FISSION CHAMBER

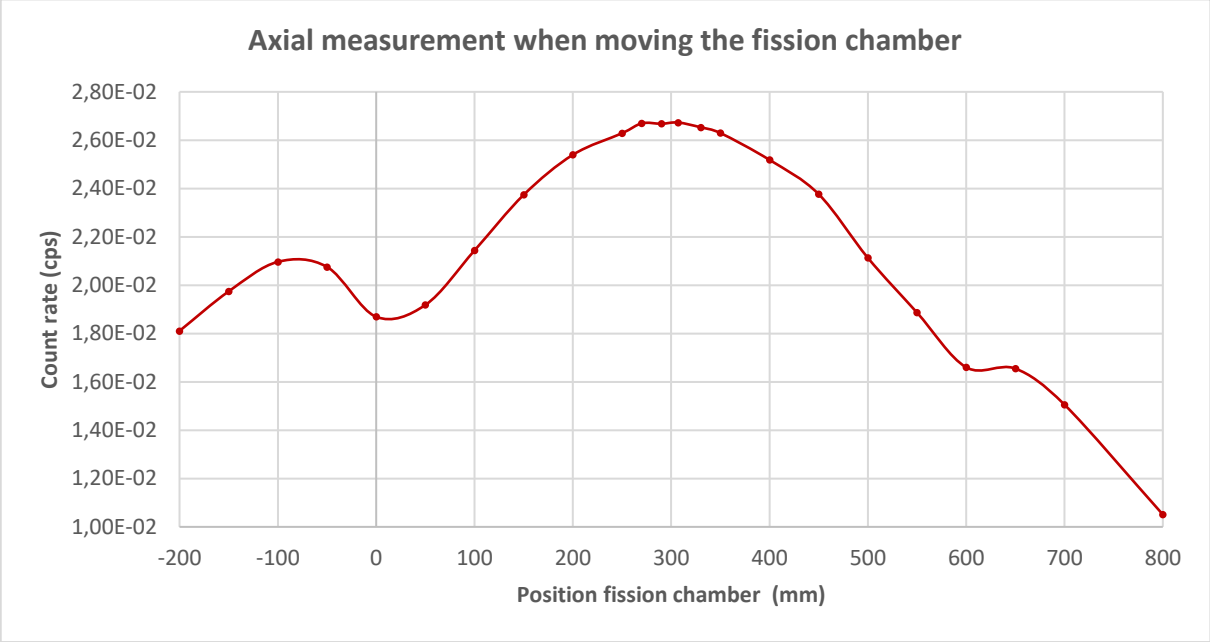

Figure 46: Measured count rate when moving the fission chamber axially. The count rate was normalized to the reactor power by a monitoring detector.

Table 16: Measured count rate when moving the fission chamber axially. The count rate was normalized to the reactor power by a monitoring detector and normalized to its maximum count rate. Normalized calculated count rate with its relative uncertainty and the relative error with the measured count rate.

Height (mm)	Count rate (cps)	Monitor count rate (cps)	Norm. power count rate (cps)	Norm. count rate (cps)	Rel. Uncert (%)	Norm calculation (cps)	Rel. Uncert (%)	Rel. Error (%)
-200	592.25	32705.38	0.018	0.677	0.530%	0.721	1.3%	7%
-150	648.22	32830.85	0.020	0.739	0.507%	0.761	1.1%	3%
-100	688.20	32824.12	0.021	0.784	0.492%	0.818	1.1%	4%
-50	680.52	32784.05	0.021	0.777	0.495%	0.815	0.4%	5%
0	615.88	32946.40	0.019	0.699	0.500%	0.713	0.6%	2%
50	632.61	32977.19	0.019	0.718	0.497%	0.724	0.3%	0.9%
100	707.23	32988.83	0.021	0.802	0.485%	0.806	0.2%	0.5%
150	782.12	32945.80	0.024	0.888	0.462%	0.892	0.2%	0.5%
200	835.52	32899.48	0.025	0.950	0.447%	0.955	0.2%	0.6%
250	865.08	32909.55	0.026	0.983	0.439%	0.991	0.2%	0.8%
270	878.60	32908.13	0.027	0.999	0.436%	0.996	0.2%	-0.3%
290	880.10	32985.53	0.027	0.998	0.435%	1.002	0.2%	0.4%
307	883.09	33035.07	0.027	1.000	0.315%	1.000	0.2%	0.0%
330	876.92	33049.68	0.027	0.993	0.436%	0.998	0.2%	0.5%
350	871.75	33151.22	0.026	0.984	0.437%	0.985	0.2%	0.1%
400	835.18	33162.35	0.025	0.942	0.447%	0.944	0.2%	0.2%
450	786.77	33103.70	0.024	0.889	0.460%	0.882	0.2%	-0.8%
500	698.30	33043.27	0.021	0.791	0.489%	0.799	0.2%	1.0%
550	620.11	32866.14	0.019	0.706	0.498%	0.697	0.3%	-1.2%
600	541.41	32605.70	0.017	0.621	0.500%	0.617	0.4%	-0.6%
650	533.76	32252.80	0.017	0.619	0.500%	0.602	0.8%	-3%
700	482.39	32037.35	0.015	0.563	0.500%	0.519	0.8%	-8%
800	337.03	32063.39	0.011	0.393	0.499%	0.345	1.2%	-12%

ANNEX B:

B1 ROSSI-A IN A CRITICAL CORE

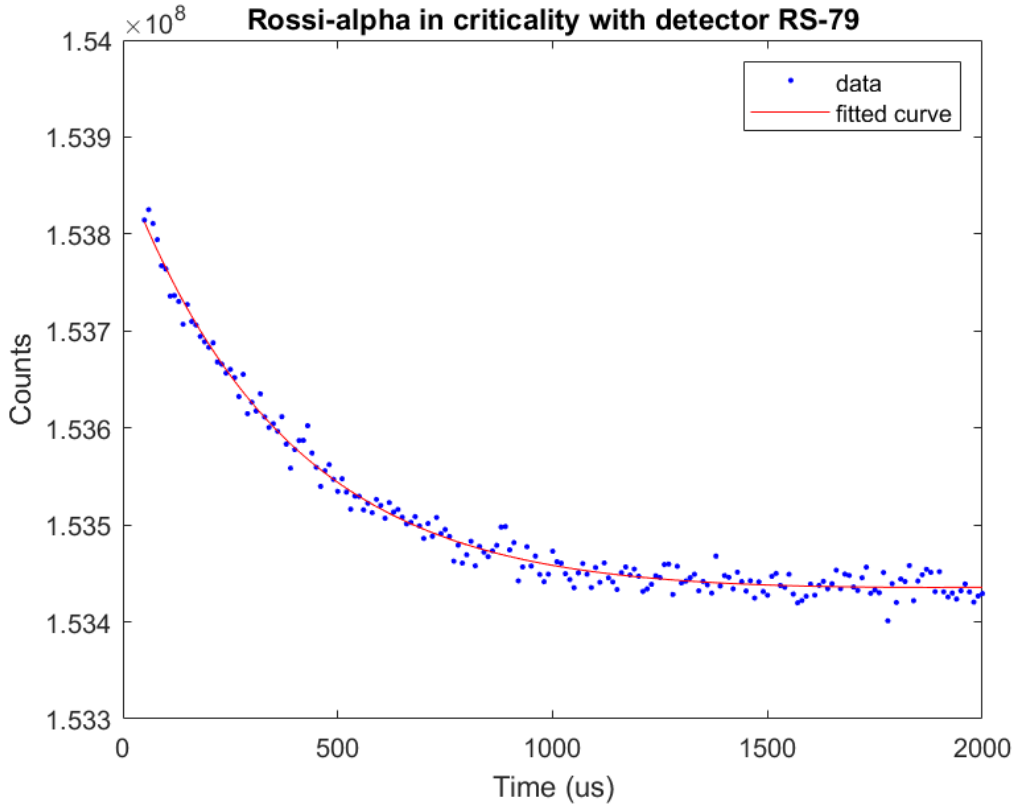

Figure 47: Fitted Rossi-α curve of data measured by detector RS_79 at day 1 in criticality.

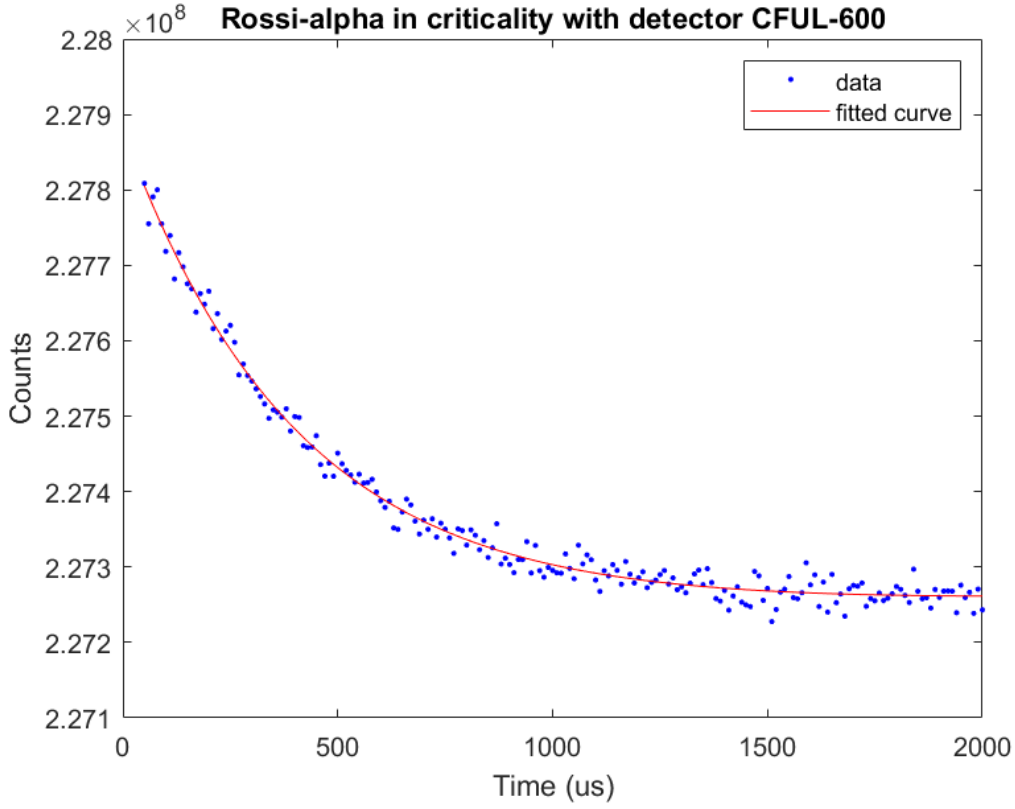

Figure 48: Fitted Rossi-α curve of data measured by detector CFUL_600 at day 1 in criticality.

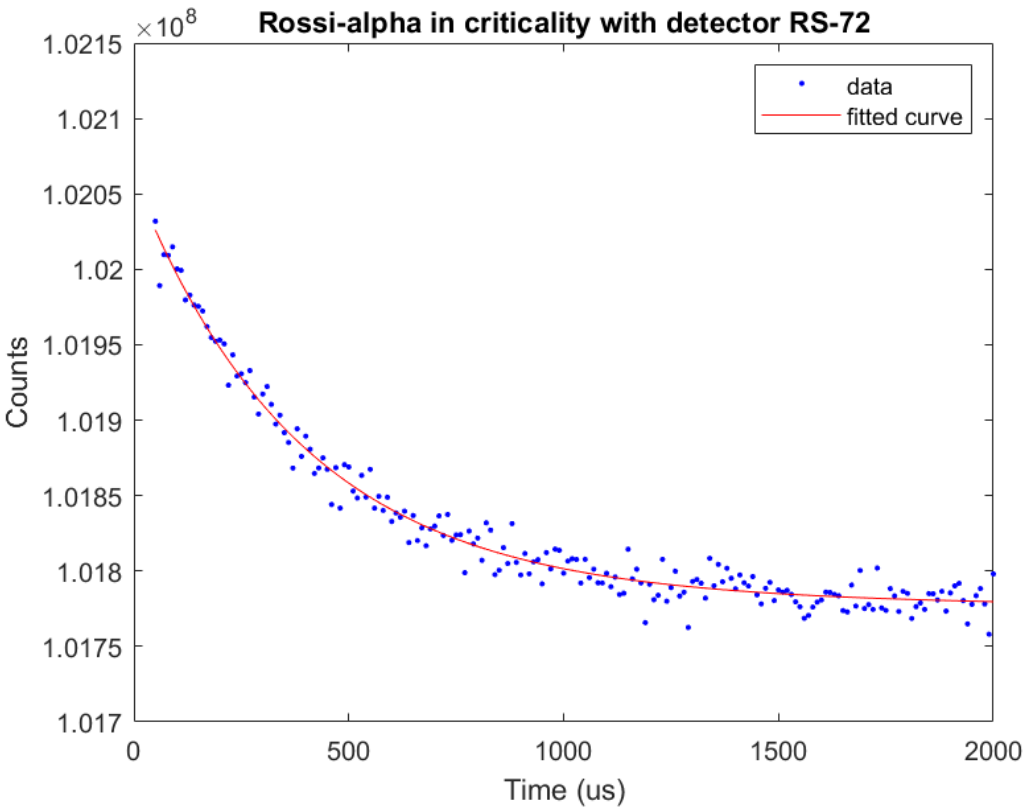

Figure 49: Fitted Rossi-α curve of data measured by detector RS_72 at day 1 in criticality.

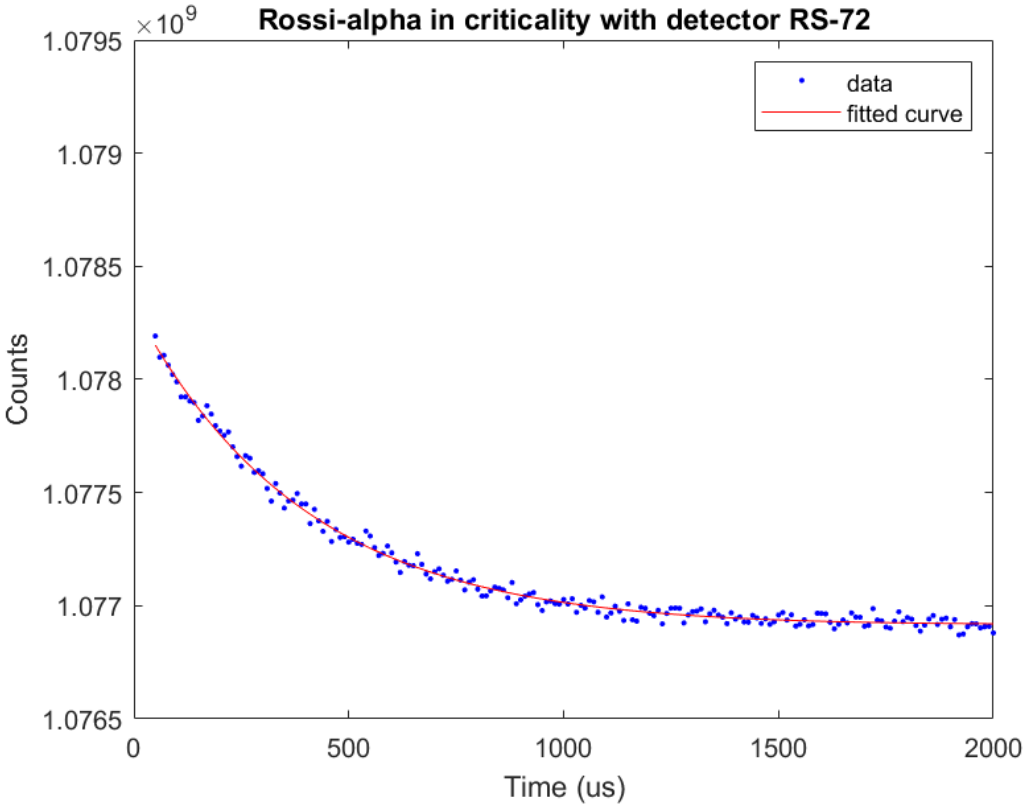

Figure 50: Fitted Rossi-α curve of data measured by detector RS_72 at day 2 in criticality.

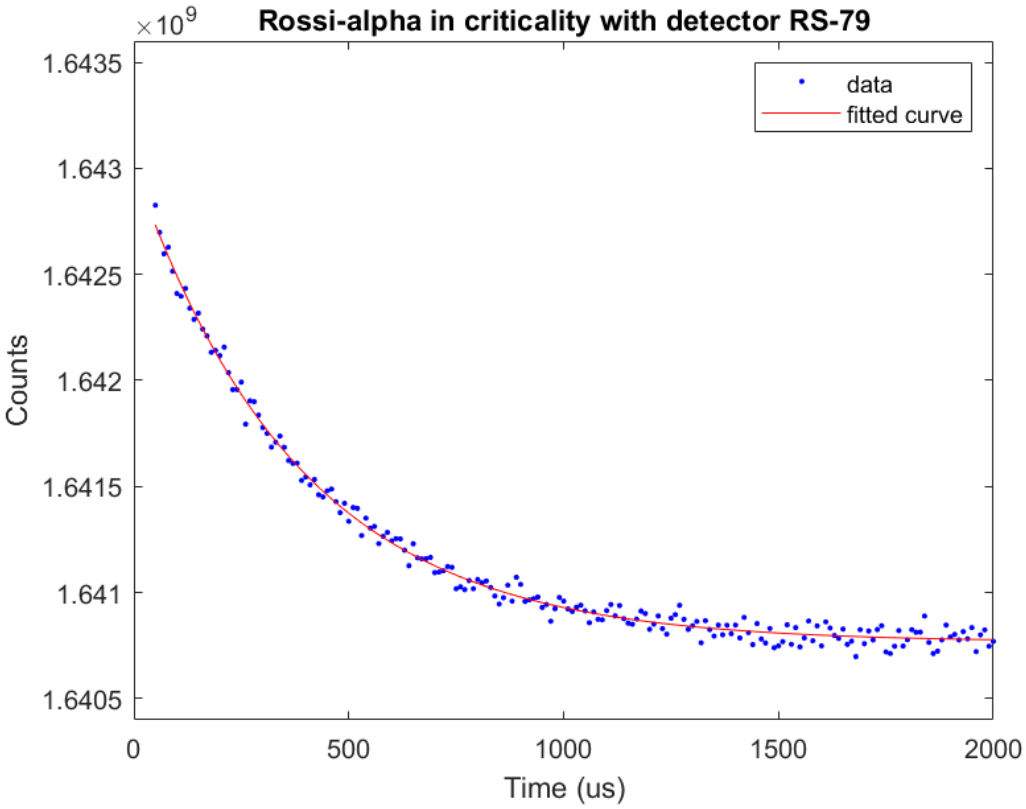

Figure 51: Fitted Rossi-α curve of data measured by detector RS_79 at day 2 in criticality.

B2 ROSSIE-A IN A SUBCRITICAL CORE

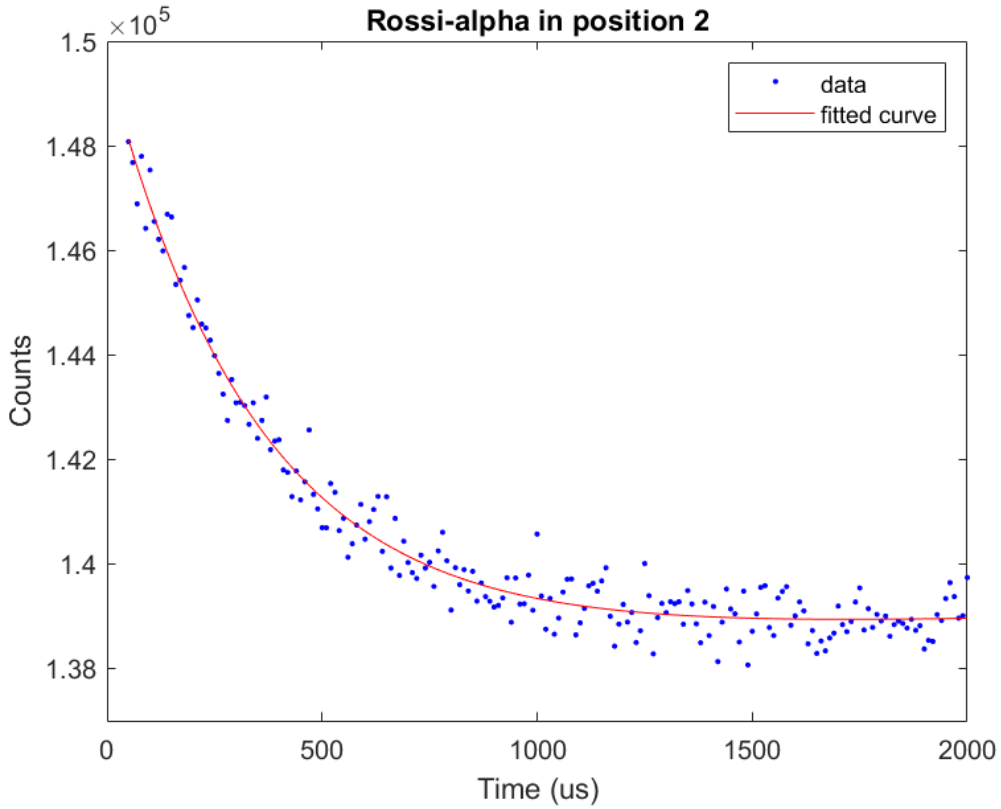

Figure 52: Fitted Rossi-α curve of data measured by detector RS_79 at day 1 in subcritical position 2 with CR1@250 and CR2@428.

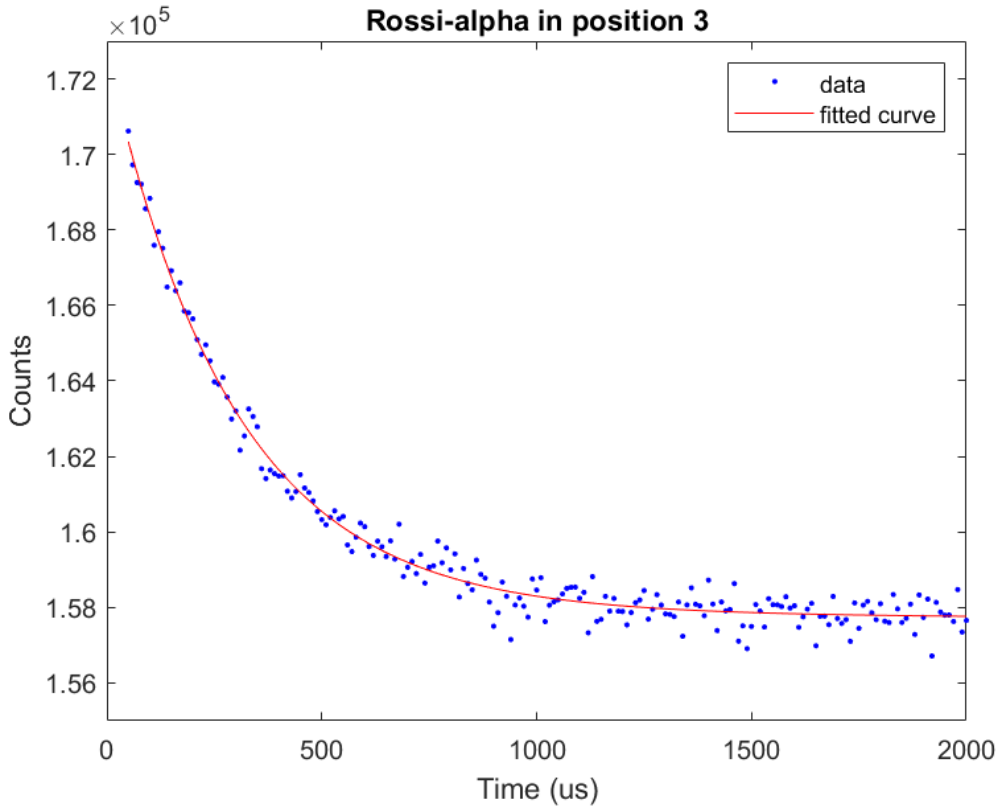

Figure 53: Fitted Rossi-α curve of data measured by detector RS_79 at day 1 in subcritical position 2 with CR1@200 and CR2@428.